

Received August 5, 2021, accepted September 15, 2021, date of publication September 29, 2021, date of current version October 7, 2021.

Digital Object Identifier 10.1109/ACCESS.2021.3116114

A Framework for Code Division Multiple Access Wireless Power Transfer

AKSHAY SARIN¹, (Member, IEEE), AND AL-THADDEUS AVESTRUZ¹, (Member, IEEE)

Department of Electrical Engineering and Computer Science, University of Michigan, Ann Arbor, MI 48109, USA

Corresponding author: Akshay Sarin (akisarin@umich.edu)

ABSTRACT The availability of energy is one of the major hindrances to unlocking the massive potential of electronic devices. Powering a highly connected network of devices requires multiple access and a wireless power transfer (WPT) solution that is scalable and capable of maintaining a constant power flow regardless of reconfiguration (mutability) and electromagnetic environment (power flow selectivity). In this paper, we present a framework for the implementation of code division multiple access wireless power transfer (CDMA-WPT) for enabling WPT among multiple transmitters and multiple receivers simultaneously. CDMA-WPT maintains power flow selectivity and is easily scalable. An inverter/rectifier topology is presented for the hardware implementation of CDMA-WPT. A design process for practical co-design of high-performance hardware and obtaining a code set is also presented. We demonstrate the hardware implementation of CDMA-WPT using two transmitters and two receivers maintaining a nearly constant 5 W operation with nearly 75 % dc-dc efficiency, and four transmitters and four receivers maintaining a constant 4 W operating with greater than 70 % dc-dc efficiency. This paper is accompanied by a video hardware demonstration in real-time the difference between using orthogonal codes in CDMA versus conventional single-frequency WPT using 4 transmitter-receiver pairs; conventional single-frequency WPT shows up to a 82 % deviation from the intended transfer power as opposed to 8.1 % for orthogonal codes in CDMA.

INDEX TERMS Wireless power transfer (WPT), code division multiple access (CDMA), current-mode class-D (CMCD), Internet of Things (IoT), power amplifier, high-efficiency, resonant converter.

I. INTRODUCTION

Wireless power transfer (WPT) is proliferating with applications that include charging of electric vehicles [1], [2], biomedical devices [3], robots [4], and electronic devices [5]. This is complemented by a rapid advancement in the fields of communication, sensing, and computation resulting in a densely connected networks of electronic devices. Realizing the full potential of these devices and applications is challenging because their functionality and performance are often limited by the availability of portable power, underscoring the need for ubiquitous wireless power.

WPT is a compelling solution to address this growing demand for power availability. To address this need for seamless power delivery, prevailing research has focused on developing efficient power delivery for single-input-multiple-output (SIMO) systems [6], [7], multiple-input-single-output systems (MISO) [8], [9], and multiple-input-multiple-output (MIMO) systems [10], [11]. The utilization of a common

electromagnetic space by multiple transmitters and receivers for power exchange is *multiple access WPT*. The transmitters (TX) and receivers (RX) participating in multiple access WPT can either have a fixed configuration with respect to each other (immutable) or can reconfigure (mutable). In this paper, the focus of the research is on the more general case of *mutable multiple access WPT*, which we will refer to as “multiple access WPT” for convenience.

A. CURRENT STATE OF THE ART

Numerous applications for multiple access WPT have been presented in the literature as we make progress towards achieving the goal of omnipresent wireless power. Examples of SIMO WPT systems include a universal contactless battery charging platform for multiple electronic devices [12], WPT for robot swarms performing various tasks in an automated environment [7], [13], [14], and WPT for unmanned aerial vehicles (UAVs) [15]. MISO systems have multiple transmitters powering a single receiver and are usually employed to improve the range, efficiency, areal coverage, and other performance factors of WPT systems. The

The associate editor coordinating the review of this manuscript and approving it for publication was Lin Zhang¹.

transmitter designs for the Qi WPT standards [16], specifically A4, A14, or A19 contain multiple transmitter coils to cover a wider area; References [5], [17], and [18] present transmitter excitation techniques for extending the physical range of WPT systems; References [19] and [20] present the use of orthogonal transmitter excitation for omnidirectional WPT. MIMO systems cover a broader category of WPT systems that allow multiple transmitters and multiple receivers to operate at the same time, taking advantage of the benefits of both SIMO and MISO systems. In [21], a MIMO system was developed to enhance the physical range of WPT that can charge multiple devices from a wireless hotspot. Reference [22] presents a Wi-power zone for extending wireless charging to multiple receivers simultaneously. In [23], a MIMO system was developed for powering distributed neural implants.

In multiple access WPT, the electromagnetic coupling between multiple TX and/or RX is unavoidable. The coupling between TX('s) and RX('s) that intentionally want to exchange power is desirable whereas all the other cross couplings are undesirable and act as sources of interference. These undesirable interferences can lead to multitudes of problems including power transfer variations, overheating of receivers, and deterioration of the system efficiency [24]. Wirelessly powered dual monitors [25], simultaneous charging of multiple electronic devices over a table [26], patients with multiple distributed implants [23], robots and drones in an autonomous environments [27] are some applications of multiple access wireless power delivery with a number of transmitters and receivers coupled to each other.

The existing techniques to achieve various types of multiple access WPT can be categorized into two fundamental approaches: non-orthogonal and orthogonal. A major difference between the two approaches is related to how multiple transmitters and receivers handle interference from each other. While orthogonal approaches avoid interference or coupling in, for example, the power signal or electromagnetic space, non-orthogonal approaches accommodate coupling or interference, through for example, feedback or optimization methods to tune the resonant circuits, hence varying the frequency, phase, or amplitude to control power transfer. Non-orthogonal methods include the use of basic compensation techniques [28], [29], analytical formulations for power maximization [30], [31], and advanced control techniques [32], [33]. For successful operation, these methods require either the use of additional communication and control circuits, intensive online computations, or accurately tuned matching networks to cancel the interference. Although non-orthogonal approaches can be a viable choice for multiple access WPT, the control complexity, computational burden, or sensitivity of these methods limits the scalability and reconfigurability, especially for mutable multiple access.

The traditional orthogonal approach for multiple access WPT involves the use of dedicated slots in time, frequency, or space for power transfer. These methods in general, do not require feedback and hence are often easier to implement.

Orthogonal methods include techniques like time division multiple access (TDMA) [25], [34], frequency division multiple access (FDMA) [35], [36], or spatial decoupling [32]. In TDMA, different TX-RX pairs take turns in exchanging power and thus use different time slots. By operating at different times, TDMA eliminates the influence of cross couplings by turning OFF the unintended TX(RX). However, for a given transceiver power rating an increasing number of TX(RX), TDMA results in lower power transfer rate. When we consider the finite range of WPT, there is an opportunity to reuse dedicated time slots. TX and RX that are physically distant enough can use the same slots without interfering. Unfortunately, reusing the slots restricts mutability. In other words, if TX and RX change their proximity, they can cause interference. A centralized controller can be used to renegotiate the slots to avoid interference and hence allow freedom of movement. However, the control complexity and the development of a strategy for centralized control is itself a nascent area of research [37], [38].

In FDMA, different TX-RX pairs use different frequency slots to allow simultaneous operation. Various multi-frequency approaches have been presented in the literature to achieve selective power transfer to multiple RX [26], [36]. However, these techniques are constrained by the limited availability of spectrum. Additionally, with a TX(RX) hardware-designed for a particular frequency the reconfigurability of the system is limited. An energy encryption approach adopted in [39] is an attractive solution for power selectivity in multiple access WPT. However, the method of dynamically switching an array of capacitors suffers from increasing hardware complexity for an increasing number of TX and RX.

Spatial decoupling can simply be attained by avoiding common electromagnetic spaces among unrelated transmitters and receivers to avert interference, but is likely impractical for mutable multiple access. Electromagnetic field cancellations such as the magnetic field editing [40], and Halbach winding arrangement presented in [41] can be used to create regions in space where magnetic fields do not interfere, enabling simultaneous operation of different TX-RX pairs. However, computation is needed for every configuration, and increasing computational complexity with larger numbers of TX and RX prevents these particular orthogonal methods from scaling well.

A potential solution to overcoming the individual limitations of TDMA and FDMA is to use frequency-hopping spread-spectrum (FH-SS) WPT [42]. FH-SS relies on changing the switching frequency (often by varying the resonant capacitance) in a pseudo-random pattern to allow users to share time and frequency slots. Scalability is limited by the number of different resonant components that can be dynamically swapped or by the range of variable capacitance.

B. POWER FACTOR IN CODE DIVISION MULTIPLE ACCESS

To overcome the limitations of TDMA and FDMA, code division multiple access (CDMA) had been employed in digital communications to improve network capacity. CDMA allows

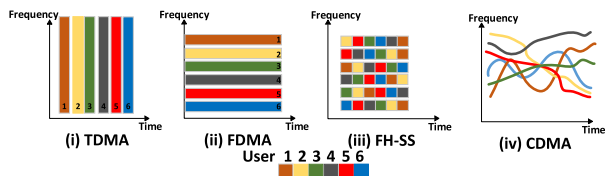


FIGURE 1. Sharing of time and frequency slots by different users: (i) TDMA only allows users to operate in different time slots; (ii) FDMA only allows different frequency slots; (iii) Frequency hopping spread-spectrum allows users to operate in pseudo-random time and frequency slots; (iv) CDMA imposes no explicitly partitioned time-frequency restrictions on users.

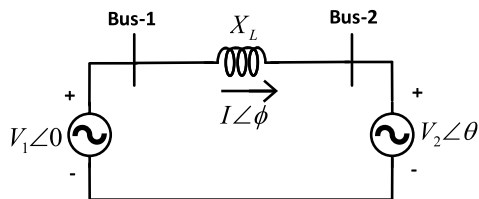


FIGURE 2. A simple power system containing two synchronous voltage sources connected through a lossless transmission line [45]. The voltages and currents are represented as phasors and the transmission line is assumed to be lossless, hence it is represented as a simple inductor.

different users to operate simultaneously on the same frequencies, at the same time, and in the same space as illustrated in Fig. 1. This is possible because CDMA, the technology behind 3G communications, relies on orthogonality in the code space to avoid interference.

Similar concepts can be used to overcome the limitations of TDMA and FDMA for WPT to deliver power via digital codes through CDMA-WPT. For mutable multiple access WPT, CDMA allows the ease of scaling while reducing the switch stress of transceivers.

The application of CDMA for WPT had previously been introduced in the following conference papers [43] and [44] by the authors. In this paper, we build on these previously introduced concepts and provide a more general framework to use CDMA for enabling power transfer in practical applications together with validation in hardware.

To understand CDMA-WPT, we extend the concept of power factor to include voltage sources encoded as digital codes. Consider a simple two-bus power system model [45], with two voltage sources, shown in Fig. 2, connected through a lossless transmission line. For this system, the two voltage sources are assumed to be sinusoidal, operating synchronously, and at the same frequency. The current through the transmission line is

$$I \angle \phi = \frac{V_1 - V_2 \angle \theta}{jX_L}, \quad (1)$$

where θ is the voltage angle of Bus-2 and X_L is the line impedance. The time-domain expressions for the voltages and the current are

$$v_1(t) = V_m \sin(2\pi ft) \quad (2)$$

$$v_2(t) = V_m \sin(2\pi ft - \theta) \quad (3)$$

$$i(t) = I_m \sin(2\pi ft - \phi), \quad (4)$$

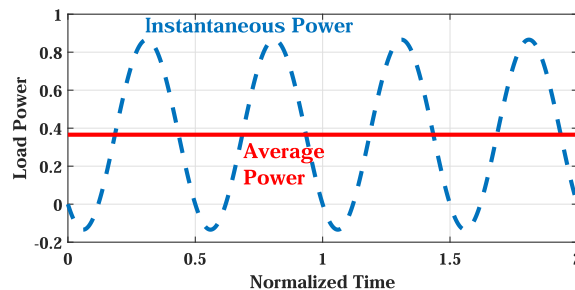


FIGURE 3. Instantaneous and average power flow from V_1 to V_2 for the simple power system model. The instantaneous power oscillates at twice the input frequency, but the average power (real power) flows from V_1 to V_2 .

where f is the frequency of operation of the power system. The instantaneous power flowing from Bus-1 to Bus-2 is

$$P(t) = v(t) \cdot i(t) = \frac{V_m I_m}{2} [-\cos(4\pi ft - \phi) + \cos \phi]. \quad (5)$$

The voltages and current in (2)-(4) are sinusoidal, making the instantaneous power (5) oscillate at twice the frequency of the voltage and current. The average power flow is given by

$$P_{\text{avg}} = \frac{1}{T} \int_{t=0}^T P(t) dt = \frac{V_m I_m}{2} \cos \phi. \quad (6)$$

The instantaneous power flow and average power flow are depicted in Fig. 3. The instantaneous power has positive and negative amplitude, with the positive instantaneous power indicating that the power flows from V_1 to V_2 , and a negative instantaneous power indicating that the power flows from V_2 to V_1 . However, positive average power indicates that over the periodic interval, the power flows from V_1 to V_2 . The factor, $\cos(\phi)$ is typically called the *power factor* of V_1 ,

$$\begin{aligned} p &= \cos(\phi) \\ &= \frac{P_{\text{avg}}}{S} \\ &= \frac{\frac{1}{T} \int_{t=0}^T v(t) i(t) dt}{V_{\text{RMS}} I_{\text{RMS}}} \\ &= \frac{\langle v_1(t), i(t) \rangle}{V_{\text{RMS}} I_{\text{RMS}}}, \end{aligned} \quad (7)$$

where ϕ is the phase difference between the voltage and the current, P_{avg} is the active power flow between the two voltage sources, $S = V_{\text{rms}} I_{\text{rms}}$ is the apparent power flow from V_1 to V_2 , and the operator $\langle \cdot, \cdot \rangle$ is the inner product [46].

It is an important generalization to consider the power factor as the inner product (7) between the time domain voltage and current. The magnitude and sign of p determine the average power flow from V_1 to V_2 ,

$$p = \begin{cases} > 0, & \text{Real power flow from } V_1 \text{ to } V_2; \\ < 0, & \text{Real power flow from } V_2 \text{ to } V_1; \\ = 0, & \text{No real power flow between } V_1 \text{ and } V_2. \end{cases} \quad (8)$$

A zero power factor means that there is no net average power flow between the buses; the two voltage sources are

thus *orthogonal* to each other. A zero power factor, however, does not mean that the instantaneous power flow between the sources is zero; rather, it implies that the instantaneous power is purely ac with no dc value. Thus, for one-half of the time period the instantaneous power flows from V_1 to V_2 and for the other half, the instantaneous power flows from V_2 to V_1 .

In wireless power transfer, the inverter/rectifier and the matching network can be replaced by equivalent voltage sources. Two voltage sources together with their coupled WPT inductors can be transformed to the two-bus voltage source model.¹ The power flow between two different voltage sources is determined by the power factor. Because power flow is bidirectional, each voltage source with its WPT inductor can behave as either a transmitter or receiver; in other words, a power electronic *transceiver*. We define *related transceivers* as those that intentionally exchange real power with each other. *Unrelated transceivers* do not transfer real power to each other. In this paper, transceivers can act as either transmitters or receivers, depending on their role in the power flow.

In CDMA-WPT, we use the concept of zero power factor to obtain orthogonal codes. We encode quasi-resonant half sine voltages (for zero voltage switching) as ternary codes (three-level); by strategically manipulating the placement of the half sine voltages, a zero power factor can be obtained. These applied voltages across the WPT inductor of each resonant transceiver governs the power flow among the transceivers. Thus, CDMA-WPT can be formulated by abstracting voltage waveforms as digital codes that determine the interactions between the transceivers. The abstraction of voltages to digital codes enables a tractable representation for finding scalable algorithms while easing the computational burden in obtaining more codes.

Power flow between transceivers can be enforced by the appropriate codes. Thus, CDMA can use code orthogonality to decouple power transfer among unrelated transceivers operating within the same electromagnetic space using similar waveforms (e.g. half sine voltages). The peak power processed by each transceiver is governed by the encoding and the number of transceivers within this shared electromagnetic space. The peak power for each transceiver is thus bounded by the maximum number of transceivers in the shared space while allowing any transceiver to have the freedom of movement through different shared spaces without the need for a centralized controller, unlike the traditional methods for multiple access WPT. Scaling the number of transceivers in CDMA-WPT is tantamount to finding digital codes that enforce the desired power flows. Thus, CDMA can help expand WPT to possibly hundreds of devices or more, making it an excellent candidate for scaling WPT.

In this paper, we present a framework for Code Division Multiple Access Wireless Power Transfer. The approach described in this paper is to the authors' knowledge, the first among methods for mutable multiple access WPT to use

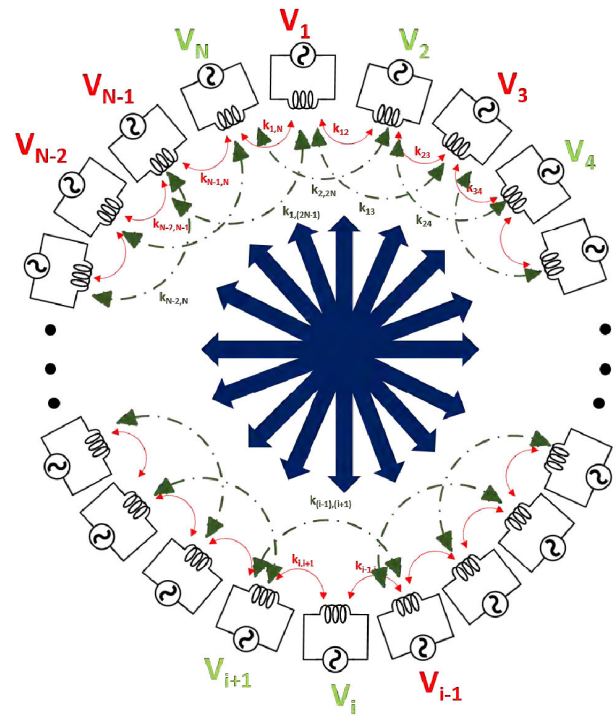


FIGURE 4. A multiple access WPT network with N transceivers: M transmitters and J receivers. Each transceiver is simultaneously coupled to multiple other transceivers.

and analyze digital encoding for wireless power transfer. To implement CDMA-WPT, a framework for digital encoding with methods to analyze the power flow between digital codes are needed. Section II introduces the digital abstraction of WPT waveforms by representing voltages or currents as ternary codes $\{-1, 0, +1\}$, along with presenting the inner-product concept of power factor to understand the power flow between digital codes. The hardware realization of these codes requires unconventional circuit topologies for the transceivers. Section III presents a soft-switching transceiver for realizing the ternary codes with bidirectional power flow capability. Analysis techniques for the transceiver are presented to show the performance and capability trade-offs in the implementation of CDMA-WPT. Section IV presents a design methodology for assembling CDMA-WPT networks with any number of related TX-RX pairs. Section V presents practical design examples and the hardware results of CDMA-WPT with two related TX-RX pairs and four TX-RX pairs.

II. MULTIPLE ACCESS WPT THROUGH DIGITAL CODES

The use of a shared electromagnetic space by multiple transceivers at the same time is defined as multiple access WPT. Fig. 4 represents an example of multiple access WPT with N identical transceivers with M transmitters and J receivers. If all transceivers are driven with voltage sources of identical frequency, the power flow will be dictated by the various coupling k_{ij} between transceivers, regardless of whether this power transfer is intended, even among unrelated

¹See Appendix A.

transceivers. As the configuration of transceivers, hence coupling, alters within the electromagnetic space, the power flow will also vary. CDMA-WPT enables mutable multiple access by using digital codes for power flow among the related pairs, thus achieving *power flow selectivity*. The unrelated transceivers use orthogonal (*non-interfering*) digital codes that operate simultaneously, achieving power transfer which is independent of changes within the electromagnetic space.

CDMA for WPT relies on the representation of voltage, current, or other physical quantities as digital codes. In this section, we present an example implementation of CDMA-WPT by encoding the output voltage of quasi-resonant converters as ternary codes (three level codes) using the C^D transformation [47]. Using the concepts presented in [47], we present a voltage source power flow model for near-field inductive power transfer, and the code construction algorithm (CCA) for scaling of WPT to a large number of orthogonal transmitters and orthogonal receivers.

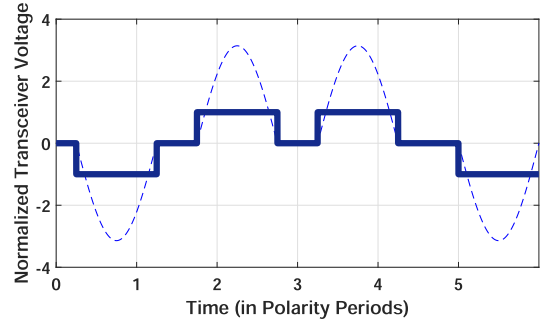
The representation of quasi-resonant voltages of a soft-switching converter as ternary codes is an effective method for obtaining a digital abstraction of the WPT voltages [43]. The C^D transformation presented in [47] is a straightforward method to represent the quasi-resonant voltages using a single ternary code voltage vector with elements $\{-1, 0, +1\}$. The C^D transformation preserves the orthogonality between two transceiver voltages, simplifies the computation for analyzing the relationship between the transceivers, and allows us to use an iterative algorithm for scaling WPT to a large number of transmitters and receivers.

The C^D transformation requires the quasi-resonant voltage to have identical amplitude and time-period, *ideal pulses*. These ideal pulses can be converted to a ternary code by first encoding the half sine voltage as square voltages of unity magnitude and then discretizing the square voltage to obtain a *ternary code*, represented by a discrete time voltage vector. The process is illustrated in Fig. 5b.

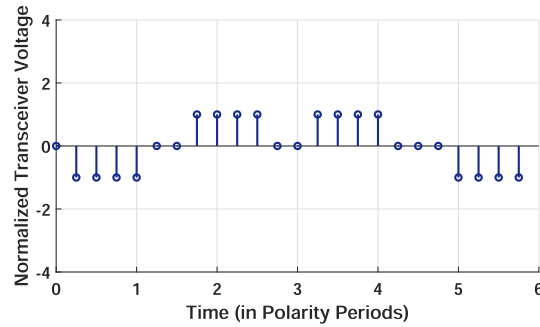
A ternary code is a discretized voltage vector with positive half sine voltages encoded as $N_P \{+1\}$ samples, negative half sine voltages encoded as $N_P \{-1\}$ samples, and the zero durations encoded using $Z_{di} \times N_P \{0\}$ samples. The choice of the number of samples N_P used to represent a polarity depends on the smallest zero duration used in the ternary code. As an example, for the ternary code shown in Fig. 5b the minimum zero duration is $\frac{1}{4}$, thus $N_P \geq 4$. The ternary code from the C^D transformation corresponding to the output voltage shown in Fig. 5b with $N_P = 4$ is

$$\mathbf{v}_1 = [\underbrace{0}_{Z_{d1}} \underbrace{\overline{1111}}_{-1} \underbrace{00}_{Z_{d2}} \underbrace{1111}_{+1} \underbrace{000}_{Z_{d3}} \underbrace{1111}_{+1} \underbrace{00}_{Z_{d4}} \underbrace{\overline{1111}}_{-1}]^T.$$

To ensure that a ternary code represents the output of the quasi-resonant transceiver in Section III, we need to enforce mathematical constraints on the ternary code vector \mathbf{v} . A ternary code \mathbf{v} is **valid** in representing the output voltage of a transceiver if:



(a) Encoding half sine voltages as square voltages of unity magnitude and the same duration.



(b) Discretization of the square voltages to obtain the ternary code vector. Each half sine voltage is represented with $N_P = 4$ samples.

FIGURE 5. C^D transformation for obtaining ternary codes from half sine voltages.

- 1) \mathbf{v} has no dc component,

$$\sum_{i=1}^l \mathbf{v}[i] = 0, \tag{9}$$

where l is the total number of samples in V .

- 2)

$$\mathbf{v}[i] \in \{-1, 0, +1\} \quad \forall i \leq l. \tag{10}$$

- 3) \mathbf{v} has intact square pulses only. An intact square pulse will contain exactly N_P consecutive $\{+1\}$ samples or exactly N_P consecutive $\{-1\}$ samples. A ternary code not having all square pulses intact is invalid. As an example for ternary codes with $N_P = 2$,

$$\mathbf{a} = [0 \ +1 \ 0 \ -1 \ -1 \ 0 \ +1]^T$$

is not a valid code; whereas

$$\mathbf{b} = [0 \ 0 \ \underbrace{-1 \ -1}_{-1} \ 0 \ \underbrace{+1 \ +1}_{+1}]^T$$

is a valid code.

The set of all valid codes will be called a **valid code set** and will be denoted by \mathbb{V} .

Definitions for Characterizing Ternary Codes:

- The ternary codes represent the long periodic switching pattern of a quasi-resonant transceiver; in other words, the pattern repeats itself after a fixed time interval. The

complete period of the ternary code is called the *code period*, and will be denoted as T .

- The time interval occupied by the half sine voltages is called the *polarity period* T_p .

A. POWER FLOW MODEL WITH DIGITAL CODES

The power flow in a conventional WPT system can be understood using the simplified voltage source model shown in Fig. 6a. The compensation network and inverter/rectifier of the two interacting transceivers are represented as equivalent voltage sources driving the two coupled WPT inductors. Appendix A derives the voltage source model for WPT. Using the Thevenin equivalent circuit at the terminals of Transceiver 2

$$i_2(t) = \int_0^t \frac{kv_1(t) - v_2(t)}{L_{Th}} dt = i_{21}(t) + i_{22}(t), \quad (11)$$

where k represents the coupling between the two WPT inductors, L_{Th} is the leakage inductance, $i_{21}(t)$ is the current contribution of Transceiver 1, and $i_{22}(t)$ is the current contribution of Transceiver 2. The average power transferred from Transceiver 1 to Transceiver 2 is

$$P_{avg} = \langle kv_1(t), i_2(t) \rangle = \frac{1}{T} \int_0^T kv_1(t) i_2(t) dt = \frac{1}{T} \int_0^T (kv_1(t) i_{21}(t) + kv_1(t) i_{22}(t)) dt, \quad (12)$$

where the operator $\langle \cdot, \cdot \rangle$ is the inner product defined over the code period, T is the code period of the transceiver codes realized by the two transceivers, k is the coupling coefficient between transceivers, $\{v_1, v_2\}$ are the voltages for Transceiver 1 and 2, and i_2 is the Transceiver 2 current. Because the model is lossless, the component $i_{21}(t)$ will only contribute to the reactive power and will not affect the average (real) power. The **power factor** of Transceiver 1 is

$$p_{12} = \frac{\langle v_1(t), i_{22}(t) \rangle}{\|v_1\|_2 \|i_{22}\|_2}, \quad (13)$$

where $\|\cdot\|_2$ is the 2-norm that represents the rms value of the waveforms over the code period. The power factor governs the power flow direction between two transceivers; if $p_{12} > 0$, power flows from Transceiver 1 to Transceiver 2 and if $p_{12} < 0$, power flows from Transceiver 2 to Transceiver 1. If $p_{12} = 0$, there is no power exchange between the two transceivers, hence the transceivers are **orthogonal**.

1) NORMALIZED POWER FLOW IN THE C^D DOMAIN

To obtain the normalized power flow in C^D , we need to determine the current vector corresponding to the ternary codes in the periodic steady state. The current vector in the

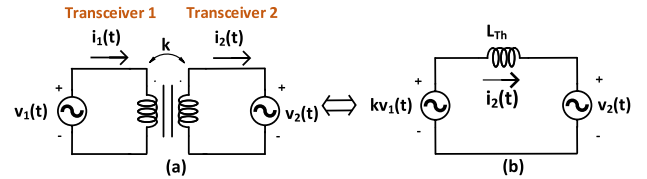


FIGURE 6. (a) Voltage source model for WPT; (b) Receiver-side Thevenin equivalent circuit for steady-state power flow analysis. $v_1(t)$ and $v_2(t)$ are the voltages of the transmitter and the receiver, respectively; L_{Th} is the leakage inductance from the perspective of Transceiver 2. $v_1(t)$ and $v_2(t)$ are half sine voltage sources with variable zero durations defined by the corresponding ternary codes.

C^D domain over the code period can be expressed as

$$i_{22} = -\frac{1}{L_{Th}} \begin{bmatrix} 1 & 0 & \dots & \dots & 0 \\ 1 & 1 & 0 & \dots & 0 \\ 1 & 1 & 1 & \dots & 0 \\ \vdots & & & & \\ 1 & 1 & 1 & \dots & 1 \end{bmatrix} \mathbf{v}_2 = \mathbf{A} \mathbf{v}_2, \quad (14)$$

where the matrix \mathbf{A} represents the integration operation in the C^D domain. \mathbf{A} maps a ternary code $\mathbf{v} \in \mathbb{V}$ with N samples to its corresponding current vector, $\mathbf{i} \in \mathbb{R}^N$. Using (14) the power factor between two transceivers in the C^D domain can be computed as

$$p_{12} = \frac{\langle \mathbf{v}_1, \mathbf{A} \mathbf{v}_2 \rangle}{\|\mathbf{v}_1\|_2 \|\mathbf{A} \mathbf{v}_2\|_2}, \quad (15)$$

where \mathbf{v}_1 and \mathbf{v}_2 are ternary codes corresponding to Transceivers 1 and 2, respectively.

B. ORTHOGONAL TRANSCIEVERS

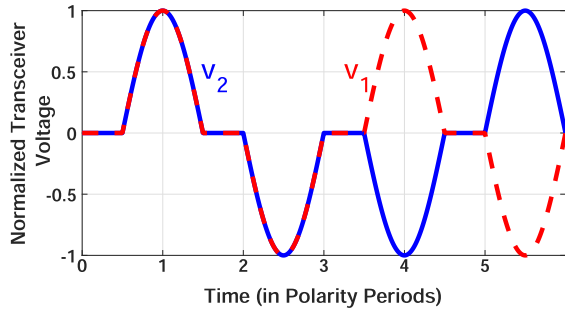
An important characteristic for effective multiple access WPT is power flow selectivity, i.e. a transmitter should only transfer power to its related receiver(s). To enable power flow selectivity with multiple transmitters and receivers in the same electromagnetic space, we require unrelated TX-RX pairs to be orthogonal. Two transceivers are said to be orthogonal if there is no average power exchange between them, thus they have a zero power factor. In this section, a method for obtaining orthogonal codes is described.

Let \mathbf{v}_1 be a given ternary code for a transceiver. A ternary code \mathbf{v}_2 that is orthogonal to \mathbf{v}_1 can be obtained by the following optimization²

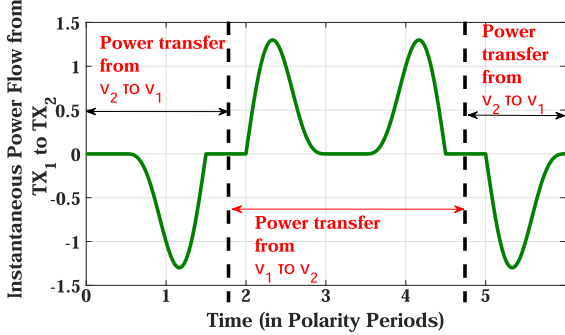
$$\begin{aligned} & \underset{\mathbf{v}_2}{\text{minimize}} && |p_{12}| \\ & \text{subject to} && \mathbf{v}_2 \in \mathbb{V}, \\ & && \|\mathbf{v}_2\|_1 = \|\mathbf{v}_1\|_1, \end{aligned} \quad (16)$$

where p_{12} is the power factor between the two transceivers, $\|\cdot\|_1$ is the 1-norm, and \mathbb{V} represents the set of valid ternary codes. The first constraint ensures that the discretized ternary

²In practice, codes can be considered orthogonal if the magnitude of the power factor p_{12} is below some chosen threshold ϵ .



(a) Ideal transceiver voltages corresponding to the two orthogonal codes (17) and (18).



(b) Instantaneous power transfer between two transceivers using (17) and (18).

FIGURE 7. Instantaneous power exchange between two orthogonal transceivers. The power factor is positive for certain durations implying that power is transferred from TX₁ to TX₂, and for durations where power factor is negative, the power flows in the other direction. The average power exchange, hence the average power factor over the code period is zero.

codes represent realizable transceiver voltages, and the second constraint ensures that Transceiver 2 has the same number of polarities (half sine voltages) as Transceiver 1. This optimization problem is non-convex, so global optimizers like the genetic algorithm (GA) can be used to obtain a solution. For an illustration, consider a simple ternary code,

$$\mathbf{v}_1 = [0 \underbrace{+1 \ +1}_{+1} \ 0 \ \underbrace{-1 \ -1}_{-1} \ 0 \ \underbrace{+1 \ +1}_{+1} \ 0 \ \underbrace{-1 \ -1}_{-1}]^T. \quad (17)$$

Using GA, we solve the optimization problem (16) to obtain a ternary code:

$$\mathbf{v}_2 = [0 \ \underbrace{+1 \ +1}_{+1} \ 0 \ \underbrace{-1 \ -1}_{-1} \ 0 \ \underbrace{-1 \ -1}_{-1} \ 0 \ \underbrace{+1 \ +1}_{+1}]^T. \quad (18)$$

Fig. 7a shows transceiver time-domain waveforms corresponding to these two orthogonal ternary codes, \mathbf{v}_1 and \mathbf{v}_2 . Although the two orthogonal transceivers have zero average power exchange over the code period, the instantaneous power exchange is not zero at all times, which can be observed in Fig. 7b.

The optimization in (16) describes a method for obtaining a code that is orthogonal to a given transceiver ternary code. However, as discussed earlier, the optimization problem is non-convex and although it may be possible to solve the problem, this method is not easily scalable. To overcome this limitation, a simple code construction algorithm (CCA) was

presented in [47]. CCA is summarized in Appendix B. The CCA starts with two orthogonal codes, and using repeated concatenation operations obtains more orthogonal codes.

C. RECEIVING POWER FROM A TERNARY CODE

To receive power from ternary codes, switched receivers that realize ternary codes are required [48]. CCA provides an efficient means to obtain a desired number orthogonal codes. These orthogonal codes can be used as transmitter codes for assembling a multiple access WPT network. To complete the system, related receiver codes are required to enable power transfer from these orthogonal transmitter codes. The receiver codes corresponding to the transmitter codes must have the following properties:

- 1) The codes must be **valid** in the sense that is described in Section II. This ensures that the receiver codes can be realized by the hardware transceiver described in Section III.
- 2) The receiver codes should seek to maximize the power from its related transmitter code, but should be orthogonal to unrelated transmitter codes.
- 3) The codes must be orthogonal to all other receiver codes.

The receiver codes satisfying the properties above are called *valid receiver codes*. These valid receiver codes help ensure power flow selectivity by only receiving power from their related transmitter codes while maintaining orthogonality with unrelated transceivers that are in proximity. The valid receiver codes therefore must have two key properties: 1) orthogonality; 2) capability of receiving power.

For the special case with $Z_d[i] \geq \frac{1}{2}$ and using receiver codes that are time-shifted versions of the related transmitter codes, a set of orthogonal transmitter codes easily results in a set of orthogonal receiver codes, with receiver codes being orthogonal to all unrelated transmitter codes [47]. Additionally, since the zero durations are constrained to the set $\{Z_d[i] \geq \frac{1}{2}, \forall i = 1 \dots M\}$, a time-shifted receiver consisting of a related transmitter waveform time-shifted by $0.5 T_p$ maximizes the power received as illustrated in Fig. 8. In the C^D domain, the shifted receiver codes have a linear relationship to their related transmitter ternary codes:

$$\mathbf{v}_R = \mathbf{S} \mathbf{v}, \quad (19)$$

where \mathbf{v}_R is the receiver ternary code corresponding to the transmitter code \mathbf{v} and \mathbf{S} is a matrix that creates a time-shift.

D. MUTABLE MULTIPLE ACCESS WPT USING CDMA

CDMA enables multiple access WPT to scale for an increasing number of transceivers with mutable configurations offering compelling advantages over other conventional methods. These transceivers operate in a shared electromagnetic space simultaneously with an appropriate choice of ternary codes to restrict power transfer only among related transceivers. In other words, the unrelated transceivers do not exchange any power despite inhabiting the same electromagnetic space.

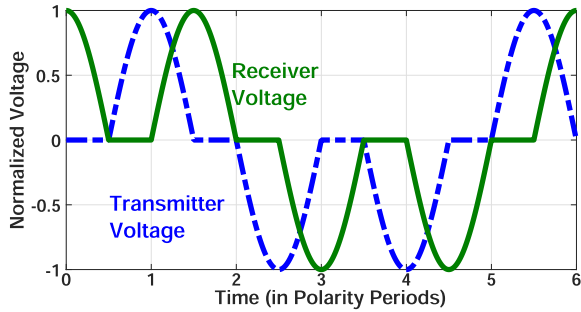


FIGURE 8. A $0.5T_p$ time-shifted receiver that maximizes power received from its corresponding transmitter while maintaining orthogonality to other unrelated receivers and transmitters.

Thus, CDMA helps to create a WPT network with dedicated power transfer among related transceivers only. These related transceivers can be either a TX-RX pair, or form sub-network with multiple TX and single RX (MISO system) or single TX and multiple RX (SIMO system).

The CCA offers a straightforward method to obtain both the appropriate transmitter and receiver codes to create a multiple access network. We can do this by choosing $Z_d \geq \frac{1}{2}$ and using a time-shift for the receiver codes. The transmitters and receivers participating in multiple access satisfy the following properties:

- 1) There is no average power exchange among the unrelated transmitters,

$$p_{ij}^T = 0 \quad \forall i \neq j \leq N, \quad (20)$$

where N is the number of unrelated transmitters, p_{ij}^T is the power factor between the i^{th} and the j^{th} transmitter.

- 2) There is no average power exchange among unrelated receivers,

$$p_{ij}^R = 0 \quad \forall i \neq j \leq J, \quad (21)$$

where J is the number of unrelated transmitters, p_{ij}^R is the power factor between the i^{th} and the j^{th} receiver.

- 3) All TXs and RXs exhibit *power flow selectivity*, which means that there is no power flow between the i^{th} transmitter and an unrelated j^{th} receiver

$$p_{ij}^{\text{TR}} = 0 \quad \forall i \neq j \leq N, \quad (22)$$

and the power flow between the i^{th} transmitter and its related receiver k^{th} is maximized,

$$p_{ik}^{\text{TR}} = p^* \quad \forall i \leq N, \quad (23)$$

where p^* is the maximum achievable power factor between a related TX-RX pair.

To evaluate the performance of CDMA-WPT in assembling WPT network, consider the simple case of with $N \times N$ network with N identical transmitters and N identical receivers, we examine the normalized power transfer rate as the number of TX-RX pairs increase. The normalized power transfer rate is the ratio of power transfer of TX-RX pairs within multiple access to TX-RX pairs in isolation for a

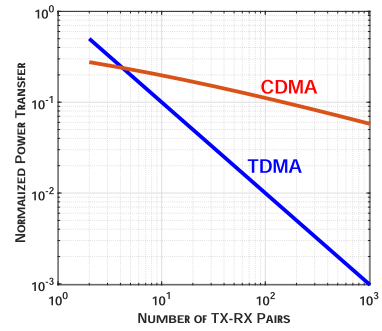


FIGURE 9. Normalized power transfer comparison for TDMA and CDMA. For TDMA, the power transfer varies inversely with the number of TX-RX pairs, i.e. $\propto 1/N$, whereas for CDMA the power transfer degrades more slowly.

given transceiver rating. Fig. 9 shows a comparison between CDMA and TDMA.

In TDMA, the N TX-RX pairs take turns through assigned time slots to exchange power. For the same transceiver ratings (i.e. identical peak power) the power transfer rate for TDMA decreases linearly $\propto 1/N$ with the number of TX-RX pairs because the duty-cycle for power transfer for each pair decreases in the same way. In addition, there is a need for a global coordination strategy to assign time slots.

For CDMA, the power transfer rate depends on the coupling among all the transceivers. Realistically, a transceiver can only be well-coupled ($k \geq 0.1$) to a limited number of transceivers, which demarcates the *region of influence* of a transceiver. With each transceiver occupying a finite physical volume, the coupling to additional transceivers decreases as the number of transceivers increases; the rate of decrease is governed by diminishing magnetic field with distance. In Fig. 9, a conservative assumption is that the coupling between the transceivers decreases linearly with distance, $k \propto 1/r$, where r is the distance. Despite this conservative model for coupling, CDMA outperforms TDMA as the number of TX-RX pairs increases.

III. TRANSCIVERS FOR CDMA-WPT

CDMA-WPT requires transceivers that can realize ternary codes. In this section, we present the analysis and design of a transceiver hardware implementation with a topology that can behave as either an inverter or active rectifier for CDMA-WPT.

The transceivers used for CDMA-WPT must necessarily have the following characteristics:

- Realize ternary codes for arbitrary polarity vectors with both positive and negative half sine voltages placed in any order.
- Realize a zero duration vector with arbitrary zero durations. It can be shown that in order to create zero durations of arbitrary size, it is necessary to freeze (hold constant) a transceiver state. Without the ability to freeze the transceiver state, only zero durations that are integer multiples of the polarity period are possible (i.e. $Z_{\text{di}} = nT_p$), where $n \in \mathbb{Z}$.

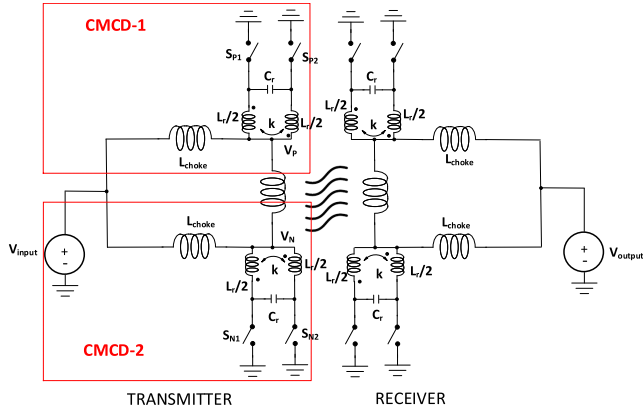


FIGURE 10. Extended CMCD (X-CMCD) topology for realizing arbitrary ternary codes. CMCD-1 can be used for creating a positive half sine voltage +1 and CMCD-2 can be used for creating a negative half sine voltage -1.

- Zero-voltage switching (ZVS) from no load to full load to achieve high efficiency at high frequency operation.

Because the receivers must also be capable of realizing ternary codes, the rectifiers must necessarily be active [48]. Additionally, having the same circuit topology for the inverter and rectifier enables the transmitters and receivers to switch roles as needed. Thus, these transceiver circuits have bidirectional power flow capability with the direction of power flow being determined by the ternary codes. Bidirectional power flow capability enables more possibilities in the creation of ad-hoc WPT networks [47].

Current-mode topologies are advantageous for the realization of ternary codes due to their ease in achieving ZVS and their ability to hold current constant in between resonant half sine voltages, hence freezing the state. The current-mode class-D (CMCD) [49] is a resonant converter topology that can realize ternary codes. However, this traditional CMCD topology is restricted to ternary codes with alternate positive and negative half sine voltages. Fig. 10 shows an extended CMCD (X-CMCD) topology acting as transmitter and receiver that overcomes this constraint [43]. The X-CMCD topology consists of a WPT inductor connected to two CMCD subcircuits with parallel resonant tanks and push-pull switches. One of the CMCD subcircuits, CMCD-1 in Fig. 10, realizes positive half sine voltages +1 across the WPT inductor; CMCD-2 realizes negative half sine voltages -1.

A. REALIZATION OF TERNARY CODES USING X-CMCD TRANSCEIVER

An X-CMCD transceiver is capable of realizing a ternary code with arbitrary patterns of positive and negative half sine voltages and zero durations. During a zero duration all four switches are closed and the currents of all the inductors are held constant. Hence, during a zero duration all the states are frozen. In the analysis, we assume all the X-CMCD components are ideal, unless otherwise specified.

To realize a positive half sine voltage +1, one of the switches S_{p1} of CMCD-1 is opened, and the CMCD-1

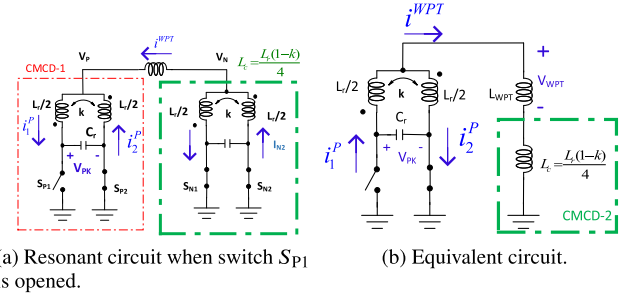


FIGURE 11. The equivalent circuit during realization of a +1 polarity using the X-CMCD transceiver. The capacitor of CMCD-1 resonates with the inductor combination to create a half sine voltage that realizes positive polarity. CMCD-2 with both its switches closed behaves as an inductor L_C . This inductor in series with the WPT inductor appears in parallel with one of the inductors of CMCD-1.

capacitor resonates with the inductor combination. Fig. 11 shows the equivalent circuit during the resonance for creating a positive polarity +1. With both switches closed, CMCD-2 behaves as an equivalent inductor with common-mode inductance $L_C = L_r(1 - k)/4$, where k is the coupling between the CMCD inductors, and $L_r/2$ is the value of each inductor. This equivalent inductance L_C is in series with the WPT inductance as shown in Fig. 11b. Using the equivalent circuit in Fig. 11b, the resonating inductance is

$$L_{eq} = \frac{(1+k)\gamma + \frac{1}{2}(1-k)}{(1+k)\gamma + \frac{1}{4}(3-k)} L_r(1+k) = l_{eq} L_r, \quad (24)$$

where k is the coupling between the CMCD inductors, and

$$\gamma = \frac{L_{WPT}}{L_r(1+k)}.$$

From (24), it can be observed that coupling the CMCD inductors increases the equivalent inductance; thus for real inductors, there is a potential for increasing the quality factor [44]. An increase in coupling coefficient leads to an increased resonating inductance; a magnetic core or interleaving techniques can increase the coupling coefficient of the CMCD tank inductors. However, one has to be wary of the additional loss mechanisms (e.g. core loss and proximity loss) associated with these techniques.

The equivalent capacitance of the resonating circuit is

$$C_{eq} = C_r + C_{sw}, \quad (25)$$

where C_r is the external capacitor and C_{sw} is the switch output capacitance. Thus, the transceiver absorbs the switch parasitic capacitance in the resonance. The equivalent capacitance and inductance determine the undamped resonant frequency ω_r and polarity period $T_P = \pi/\omega_r$ of the ternary code.

The peak magnitude of capacitor voltage V_C is related to the current of the corresponding inductor $i_1^p(0)$ just before the switch operation.

$$V_C \approx \sqrt{\frac{L_{eq}}{C_{eq}}} i_1^p(0), \quad (26)$$

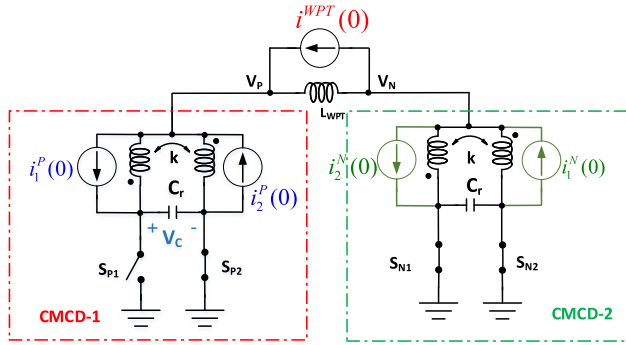


FIGURE 12. The current distribution among inductors just before the switch S_{p1} is turned OFF. The peak voltage across the capacitor during the resonance is related to the initial current in the corresponding inductor $i_1^P(0)$ before the operation of the switch.

where L_{eq} is the equivalent resonating inductance and C_{eq} is the equivalent resonating capacitance. $i_1^P(0)$ is the current in the inductor just before opening of switch S_{p1} as illustrated in Fig. 12. The amplitude of the half sine voltage is thus dependent on the current distribution among the inductors during the preceding zero duration.

For the realization of positive half sine voltages, the switches of CMCD-1 can be opened alternately with both switches on CMCD-2 closed and vice-versa for negative half sine voltages. Thus, a ternary code determines the switching sequence of an X-CMCD transceiver.

Given a ternary code, we can estimate the steady-state currents and voltages for the X-CMCD transceiver using simple linear equations based on the fundamental properties of volt-second balance across the choke inductors and periodicity of the currents over the code period (see Appendix C). These steady-state currents and voltages, referred to as the *model waveforms* will be used for analysis and design of the X-CMCD transceivers.

B. TRANSFER POWER

The *transfer power* is defined as the power transferred between transceivers in WPT. In the following sections, transfer power P_{TR} will be restricted specifically from the transmitter to the receiver; using the calculated currents and voltages of the transmitter and the receiver

$$P_{TR} = \frac{1}{T} \int_0^T v'_{TX}(t) i_{RX}(t) dt, \quad (27)$$

where $v'_{TX}(t)$ is the instantaneous voltage across the transmitter WPT inductor reflected to the receiver side; $i_{RX}(t)$ is the instantaneous current of the receiver WPT inductor; and T is the code period. The voltage across the WPT inductor is related to the voltage of the resonating capacitor

$$\begin{aligned} v_{WPT}(t) &= v_P(t) - v_N(t) \\ &= \frac{\gamma(1+k)}{\gamma(1+k) + \frac{1}{2}(1-k)} \frac{v_{C1}(t) - v_{C2}(t)}{2}, \quad (28) \end{aligned}$$

where $v_{C1}(t)$ and $v_{C2}(t)$ are the voltages across the resonating capacitors of CMCD-1 and CMCD-2, respectively. Note that

for a given polarity, either but not both v_{C1} or v_{C2} are nonzero. From (28), it can be observed that for large γ , the voltage across the WPT inductor is $\approx v_C/2$. The voltage across and current through the WPT inductor depends on the ternary code and the ratio γ .

Transfer power can be expressed as

$$P_{TR} = \kappa_{tr} V_n I_n, \quad (29)$$

where κ_{tr} depends on the ternary code; V_n and I_n are the nominal voltage and current for the constant amplitude half sine voltages and currents of a CMCD subcircuit for a ternary code with alternating polarities. κ_{tr} is a constant that captures the characteristics of the different ternary codes, while the nominal voltage and current represent the hardware ratings. Thus, the transfer power is expressed as a product of a quantity that depends on ternary codes κ_{tr} and the voltage and current ratings of the transceiver. The nominal transceiver voltage and current are related by equation (26).

C. TRANSCEIVER LOSS ESTIMATION

In order to design efficient X-CMCD transceivers we need to estimate the dc-dc efficiency with CDMA-WPT, hence the resulting losses in the transceivers. The transceiver model waveforms can be used for calculating the losses in a WPT system.

For an unloaded X-CMCD transceiver in isolation, the voltages and currents depend primarily on the input dc voltage, component reactances, and the ternary code. Thus, for a well-designed transceiver the losses are small; otherwise, losses are dependent on the operating point of the transceiver. For loose coupling between two X-CMCD transceivers, the losses are also nearly that of the isolated X-CMCD. Hence, for the estimation of end-to-end efficiency and the evaluation of ternary codes for low-loss, loosely-coupled X-CMCD transceivers, the unloaded losses can be used. It is worth noting that, in general for ternary codes, the voltage and current waveforms do not have only a single frequency component, hence the loss calculations for the hardware implementation of CDMA differ from that of conventional resonant converters used for WPT. The main sources of loss in an X-CMCD transceiver are:

- 1) *CMCD Inductor Loss*: The frequency of operation and the spectral content of the voltage and current waveforms depends on the ternary code characteristics. We can use the spectral content of the model waveforms associated with the ternary codes to estimate the CMCD inductor loss. This loss depends on the inductor realization; while higher frequency operation may favor the use of air-core inductors, the advantages of coupled CMCD inductors tend to favor the use of a magnetic core. Depending on the realization, there may be two kinds of inductor losses: core loss and conduction loss. The accurate prediction of core loss may require more advanced methods like iGSE [50] and is a topic for future research. Although the exact

value of the inductor resistance depends on the realization (e.g. air-core or magnetic-core inductor), for the purposes of design, we only model skin effect for the frequency dependence of the equivalent resistance. The approximate conduction loss is

$$P_{Lr} = \sum_{i=1}^M I_i^2 R_{fr} \sqrt{\frac{f_i}{f_r}}, \quad (30)$$

where I_i is the i^{th} frequency component of the inductor current, f_i is the i^{th} frequency, f_r is the resonant frequency, and R_{fr} is the resistance at the resonant frequency.

2) *Switch Loss*: The main loss mechanisms in the switches are the conduction loss, output capacitance loss, turn-OFF loss, and gating loss. The turn-OFF loss and gating loss are not included in this analysis as a simplification, but can conceivably be added.

- **Conduction Loss**—The switch conduction loss can be estimated by

$$P_{\text{cond}} = I_{\text{sw}}^2 R_{\text{DS}}, \quad (31)$$

where I_{sw} is the rms switch current and R_{DS} is the on-resistance of the switch.

- **C_{OSS} Loss**—There is a loss associated with the charging and discharging of the parasitic output capacitance during resonance, even though the transceiver is soft-switched. To estimate the C_{OSS} loss, we will use the Steinmetz equation provided in [51] along with the appropriate parameters. The energy dissipated during a charge-discharge cycle of a switch can be approximated by

$$E_{\text{DISS}} = k C_{\text{OSS}} f_r^\alpha V_{\text{pk}}^\beta, \quad (32)$$

where k , α , and β are Steinmetz constants. Although, there is some intuition for determining the Steinmetz constants, the exact mechanisms and magnitude of these losses is largely a continuing topic of research [52]. However, based on the output capacitance of the switches, the upper bound of the energy dissipation can be expressed by

$$E_{\text{DISS}} \leq \frac{1}{2} b C_{\text{OSS}} V_{\text{pk}}^2, \quad (33)$$

where b is the fraction of energy dissipated by the switch. Thus, the total power loss from the output capacitance is

$$\begin{aligned} P_{\text{COSS}} &\leq \frac{1}{T} \sum_{i=1}^M \frac{1}{2} b C_{\text{OSS}} V_{\text{pk}}^2 [i] \\ &\leq \frac{b T_{\text{P}}}{T} C_{\text{OSS}} f_r \sum_{i=1}^M V_{\text{pk}}^2 [i], \end{aligned} \quad (34)$$

where $V_{\text{pk}}[i]$ is the peak switch voltage during the realization of i^{th} polarity, T is the code-period, D is the duty-cycle of the code, M is the number

of polarities in the code, and f_r is the resonant frequency.

In addition to the CMCD inductor loss and the switch loss, each transceiver also has losses in the WPT inductor, which can be lumped into the CMCD inductor loss. The choke inductor loss is designed to be low, only carrying dc current and a small ripple. There may also be circuit losses associated with high frequency parasitic ringing, which can also be minimized in a good design.

The total transceiver loss can now be expressed as the sum of the main loss components

$$\begin{aligned} P_{\text{loss}} &= P_{Lr} + P_{\text{cond}} + P_{\text{COSS}} \\ &= \sum_{i=1}^M I_{i,Lr}^2 R_{fr} \sqrt{\frac{f_i}{f_r}} + I_{\text{sw}}^2 R_{\text{DS}} \\ &\quad + \frac{b T_{\text{P}}}{T} C_{\text{OSS}} f_r \sum_{i=1}^M V_{\text{pk}}^2 [i] \\ &= \kappa_{Lr} R_{fr} I_n^2 + \kappa_{\text{cd}} R_{\text{DS}} I_n^2 + \kappa_{\text{CS}} f_r C_{\text{OSS}} V_n^2, \end{aligned} \quad (35)$$

where κ_{Lr} , κ_{cd} , and κ_{CS} are constants that depend on the characteristics of a ternary code; V_n and I_n are the nominal transceiver voltage and current.

D. END-TO-END WPT EFFICIENCY AND THE LOSS-FACTOR

Using the calculated losses in a transceiver (35) and transfer power (29), the dc-dc efficiency of the WPT system can be determined.

The receiver ternary codes are time-shifted versions of the transmitter code. Thus for loosely-coupled WPT inductors, the loss in the transmitter and receiver will be approximately identical ($P_{\text{loss,T}} \approx P_{\text{loss,R}}$). Hence the dc-dc efficiency of WPT system can be expressed as

$$\begin{aligned} \eta &= \frac{P_{\text{out}}}{P_{\text{in}}} \\ &= \frac{P_{\text{TR}} - P_{\text{loss}}}{P_{\text{TR}} + P_{\text{loss}}} \\ &= \frac{1 - \ell}{1 + \ell} \quad \text{where } \ell = \frac{P_{\text{loss}}}{P_{\text{TR}}}; \end{aligned} \quad (36)$$

$P_{\text{loss}} = P_{\text{loss,T}} = P_{\text{loss,R}}$ is the power loss in either transmitter or receiver. From (36), it can be observed that maximizing η is same as minimizing ℓ . We define the quantity ℓ as the *loss-factor* of a transceiver. Using (29) and (35), the loss-factor for a transceiver can be expressed as

$$\begin{aligned} \ell &\triangleq \frac{P_{\text{loss}}}{P_{\text{TR}}} \\ &= \frac{\kappa_{Lr} R_{fr}}{\kappa_{\text{tr}} \omega_r L_{\text{eq}}} + \frac{\kappa_{\text{cd}} R_{\text{DS}}}{\kappa_{\text{tr}} \omega_r L_{\text{eq}}} + \frac{\kappa_{\text{CS}} \omega_r^2 L_{\text{eq}} C_{\text{OSS}}}{2\pi \kappa_{\text{tr}}} \\ &= \frac{n_{Lr}}{Q_{fr}} + \frac{n_{\text{cd}} \tau_{\text{sw}}}{\omega_r L_r C_{\text{OSS}}} + n_{\text{COSS}} \omega_r^2 L_r C_{\text{OSS}}, \end{aligned} \quad (37)$$

where n_{Lr} , n_{cond} , and n_{COSS} are parameters that are dependent on the ternary code; $Q_{fr} = \omega_r L_r / R_{fr}$ is the quality factor of the CMCD inductors; and $\tau_{\text{sw}} = C_{\text{OSS}} R_{\text{DS}}$ is a parameter

dependent on the switch technology. These ternary-code-dependent parameters can be obtained from the model waveforms of the transceiver.

As will be discussed in the following section, the loss-factor is used for designing efficient transceivers for CDMA-WPT. There are certain advantages in minimizing the loss factor to obtain the transceiver parameters as opposed to maximizing efficiency:

- 1) The loss-factor is to a good approximation, independent of the input voltage (hence operating point). The transfer power is homogeneous to the input voltage, hence making the loss-factor largely independent of power. In practice, the loss-factor would be designed to be only a weak function of the operating point with a dependence related to the non-linearity of the transceiver components.
- 2) At a particular resonant frequency of operation ω_r and a fixed ratio γ , the optimization to obtain the transceiver parameters is convex in the variable $x = L_r C_{OSS}$. Thus, the optimization can be easily solved to obtain the best transceiver components using standard optimization tools while the convexity guarantees the existence of a global optimum.

For a given resonant frequency with the components designed to operate with small non-linearity, the quality factor of the CMCD inductors Q_{fr} and the switch time constant τ_{sw} are fixed, and depend on the realization of the inductors and the switch technology.

E. NUMBER OF ORTHOGONAL CODES AND TRANSFER POWER

Although the X-CMCD topology does offer the flexibility to realize ternary codes, the hardware design of the transceiver imposes constraints on the polarity vectors [44]. In this section, we discuss the hardware constraints and tradeoffs related to the realization of ternary codes by X-CMCD transceivers. Specifically, we examine the tradeoff between the total number of orthogonal codes and transfer power.

A ternary code is *realizable* if every switch turn-off creates a half sine voltage across the WPT inductor. The peak magnitude of this half sine voltage depends on the distribution of the inductor currents before the operation of the switch, as described in Section III-A. During the realization of a polarity, it is possible that the inductors of the corresponding CMCD subcircuit carry currents such that turning OFF a real-world FET leads to reverse conduction through the switch, as illustrated in Fig. 13. For example, during reverse conduction, the current flows through the body diode of a silicon MOSFET or through the channel of a reverse diode-connected GaNFET. As a result, the voltage across the capacitor will be clamped to the diode voltage and there will be no resonance. The voltage across the WPT inductor remains zero and the corresponding polarity will not be realized. Thus, an inappropriate polarity for the current distribution can lead to *code-failure*. Hence, a code-failure occurs in a transceiver

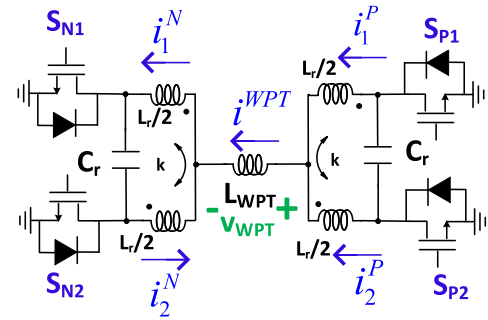


FIGURE 13. Current distribution for a transceiver before the realization of a polarity. This current distribution only allows the transceiver to have a negative polarity because turning OFF S_{P1} or S_{P2} cannot create the resonance needed for realizing a positive polarity.

when turning OFF a switch does not lead to a half sine voltage across the WPT inductor.

The current distribution in the CMCD inductors depends on the circuit parameters and the ternary code. The important circuit parameters that determine the current distribution are:

- 1) γ , which represents the ratio of energy stored in the WPT inductors to the energy stored in CMCD tanks,³ and
- 2) k , the coupling between the CMCD inductors.

The maximum achievable coupling k between the CMCD inductors is determined by the inductor realization. Thus, the factor γ primarily determines the number of ternary codes that a transceiver can realize. Fig. 14 helps understand the effect of γ on the realization of ternary codes. The figure shows the equivalent circuit of an X-CMCD transceiver during the realization of a positive polarity; hence one of the switches in CMCD-1 is opened. CMCD-2 with both switches closed is represented by an equivalent common-mode inductance L_c . This series combination of common-mode inductance with the WPT inductor appears in parallel with one of the inductors in CMCD-1. During the resonance, a part of the energy in CMCD-1 is transferred to CMCD-2 through the WPT inductor with γ determining the amount of energy that is transferred. Thus, after the realization of this polarity, the magnitude of the current $i_2^P[j + 1]$ will be less than $i_1^P[j]$. The magnitude of the half sine voltage created during the resonance depends on the current in the corresponding inductor L_{p1} before the switch is turned OFF, specifically expressed in (26). The difference between the inductor currents leads to different magnitudes of the half sine voltages with a possibility of a code-failure; because $|i_2^P| \leq |i_1^P|$, consecutive positive polarities will have different voltage magnitudes.

A small value of γ leads to more energy being transferred from one CMCD subcircuit to the other and hence a larger difference in the magnitudes of consecutive polarities, whereas a larger γ leads to a smaller energy exchange between the CMCD subcircuits and hence a smaller voltage difference between consecutive polarities as illustrated in Fig. 15. Thus, a large γ keeps the energies in the CMCD subcircuits closer

³ $\gamma = \frac{L_{WPT}}{L_r(1+k)}$.

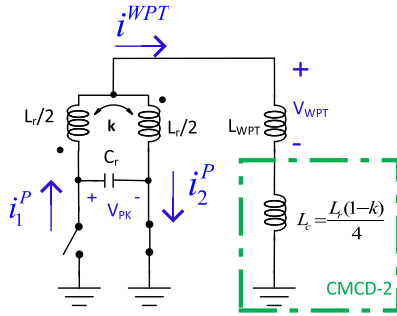


FIGURE 14. X-CMCD equivalent circuit during the realization of a positive polarity. CMCD-2 is represented using an equivalent inductance L_c .

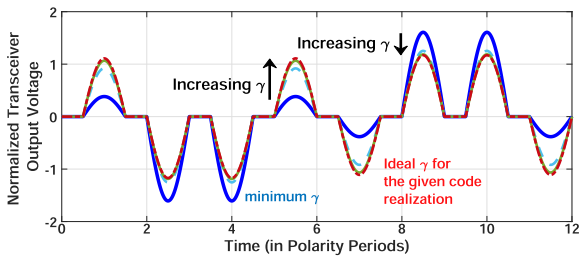


FIGURE 15. Variation of voltage across L_{WPT} with γ . For the realization of a particular ternary code, a certain minimum γ is required. However, the minimum γ leads to large variations in the peak voltage. The variations in the peak voltage decrease with increasing γ .

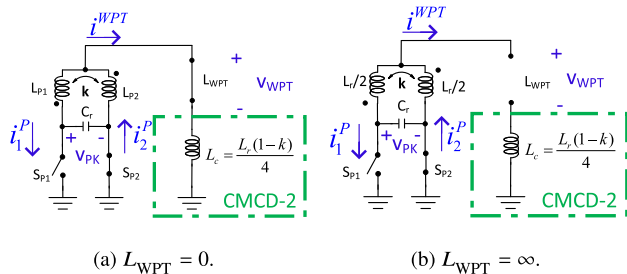


FIGURE 16. Equivalent circuit for two extreme values of γ : (a) $\gamma = 0$, WPT inductor is a short; and (b) $\gamma = \infty$, WPT inductor is an open circuit.

to constant. Hence, to create more codes and hence more orthogonal TX-RX pairs, it is advantageous to have a large γ .

Additionally, to maintain the orthogonality between the codes created using CCA, it is preferable to have ternary codes with identical half sine voltages. Orthogonality within the C^D transformation relies on the interaction between transceivers with identical half sine voltages to have zero power factor. Although a small γ can realize a ternary code, it may lead to large variations in the peak magnitudes of the half sine voltages as illustrated in Fig. 15. Variation in the magnitude of the half sine voltages can weaken the strict orthogonality between the codes, which creates unwanted power transfer between unrelated transceivers. To reduce interference and to approach ideal half sine voltages, γ must be increased. In practice, codes can be considered orthogonal if the magnitude of the power factor p is below some chosen threshold ϵ ; for the remainder of this paper, which will focus on the hardware considerations, $|p| < \epsilon$ will be considered orthogonal.

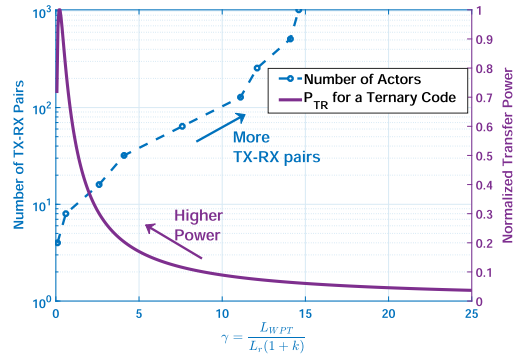


FIGURE 17. Plot showing the tradeoff between transfer power and number of orthogonal TX-RX pairs. A large γ helps to create more orthogonal codes for the TX-RX pairs, but results in smaller transfer power.

Changing γ also changes the transfer power from a transmitter to its receiver. From Fig. 16, we can observe that for a γ too large (approaching an open circuit, i.e. no WPT inductor), the transfer power from transmitter to the receiver will be zero, because there will be no receiver WPT current. Alternatively, for a γ too small, there will be negligible transfer power because of a very small transmitter voltage. Thus, for some intermediate $\gamma = \gamma_P$, the transfer power will be maximum. Hence, the maximization of transfer power requires operation at a certain γ for a particular code.

For a given orthogonal code set obtained using CCA, there is a minimum γ required to realize all the orthogonal ternary codes; there are also optimal γ that maximize the transfer power from TX to RX for each code. While the realization of codes and orthogonality benefits from higher γ , the transfer power benefits from small γ . This trade-off is depicted in Fig. 17. The minimum γ required to realize a progressively larger code set (i.e. greater number of TX-RX) can be determined numerically. The transfer power for one of the ternary codes, which is numerically calculated from model waveforms, is also plotted versus γ . Although increasing γ can help realize a large number of codes, there will be a corresponding decrease in transfer power.

IV. THE DESIGN PROCESS

The transceiver analysis in the last section, describing the behavior of voltage and current waveforms for a particular code, lays a foundation for the practical co-design of high-performing hardware and a realizable code set. In this section, we develop a design process for creating CDMA-WPT networks with any number of unrelated TX-RX pairs.

The design process begins by selecting a realizable and orthogonal (RO) code set from a candidate code set through γ . The selection of specific transceiver components L_r , L_{WPT} , C_r , and the semiconductor switch is optimized through the loss-factors of the RO code set.⁴ By using loss-factor as a proxy for efficiency, this overall optimization is convex.⁵

⁴Recall that the loss-factor model in (37) is independent of absolute power.

⁵It is worth noting that a direct optimization of power factor of the RO code set is not convex and is a topic for future research.

The voltage and currents of the transceiver depend on the inductors (L_r and L_{WPT}) and capacitor (C_r) participating in resonance. Therefore, the design space for X-CMCD transceivers consists of the following parameters: γ , semi-conductor switch, L_r , and C_r .

These parameters are chosen at the beginning of the design process:

- 1) Number of orthogonal transceivers: N
- 2) Switch technology dependent parameter: τ_{sw}
- 3) Inductor technology dependent parameter: Q_{fr}
- 4) Coupling between the CMCD inductors: k .

The design process is as follows:

Step 1: Create the candidate code set: CCA is used to obtain 2^m ternary codes, such that $m \geq N$. The minimum γ required for each code is in general different; γ_{min} is the largest minimum γ among all the codes in the candidate code set. In other words, γ_{min} is the smallest γ that realizes the entire code set.

Step 2: Ensure the orthogonality of the code set: The realizability of a code set does not guarantee that the codes are orthogonal. Using γ_{min} and model waveforms, obtain the power factor between all pairs of codes in the initial code set. Use Algorithm 1 to filter out the orthogonal codes⁶ from the initial code set. If the number of orthogonal codes is equal to or larger than N , then go to Step 3 to obtain the other transceiver parameters, if not go back to Step 1 to create a larger code set.

Step 3: Minimize the loss-factor: The next step in the design process is to choose the correct switch, CMCD inductors L_r , and resonant frequency $\omega_r(L_r, C_r, \gamma)$:

$$\text{minimize } \ell = \frac{P_{loss}}{P_{TR}} \quad (38)$$

For a fixed resonant frequency, the objective function is convex in the variable $x = L_r C_{OSS}$ and can easily be solved to obtain the values of the resonant components.

Step 4: Obtaining a better γ : Further improvements in loss-factor may be obtained by increasing γ beyond γ_{min} . For each iteration of $\gamma \geq \gamma_{min}$, a new ℓ_{min} is calculated and compared to the previous, $\ell_{min,prev}$.

The design process begins with the creation of a candidate code set with a γ_{min} that realizes all the ternary codes. However, from Section III-E, γ_{min} may lead to ternary codes with different peak magnitudes for the half sine voltages as shown in Fig. 15, so the orthogonality between codes described for the C^D transformation cannot be strictly satisfied. Instead, the power factor between all the codes in the code set can be used as a measure of interference, which below a threshold

⁶Based on a power factor threshold ϵ .

Algorithm 1: Obtaining the Orthogonal Code Set

Result: Orthogonal codes for a given γ .

Calculate infinity norm of power factor matrix a_{inf} ;

while $a_{inf} > \epsilon$ **do**

Obtain 1-norm for every column of the power-factor matrix ;

Remove the row and column corresponding to the maximum 1-norm ;

Calculate the new a_{inf} ;

end

can represent a practical orthogonality. Algorithm 1 eliminates these interfering ternary codes based on the magnitude of the interference to obtain the largest orthogonal code set. If the number orthogonal codes obtained using Algorithm 1 is fewer than the required N , then the initial code set created using CCA can be expanded to obtain additional orthogonal codes, repeating the process until N orthogonal codes are obtained.

V. HARDWARE RESULTS

To demonstrate the practical application of CDMA-WPT for creating WPT networks, design examples are presented in this section. The design examples follow the process outlined in the previous section to obtain the orthogonal ternary codes and the transceiver components.

The transceiver design is then implemented in hardware to demonstrate effective multiple access WPT. The transceivers are controlled by the same FPGA.⁷ Using hardware, we verify three main concepts related to CDMA-WPT:

- 1) Realization of appropriate ternary codes;
- 2) Receiving power from ternary codes;
- 3) Demonstrating multiple access WPT.

A. DESIGN OF WPT NETWORKS WITH FOUR TRANSCIEVERS

Consider a design example with 4 transceivers operating as two transmitters (TX₁, TX₂) and two receivers (RX₁, RX₂), thus forming a 2 × 2 WPT network. The objective is power flow selectivity so that only TX₁ can power RX₁ and only TX₂ can power RX₂, regardless of the cross coupling between the unrelated transceivers. The two transmitter codes obtained using the optimization described in Section II-B are

$$\mathbf{v}_{TX1} = [0 \ +1 \ +1 \ 0 \ -1 \ -1 \ 0 \ +1 \ +1 \ 0 \ -1 \ -1]^T,$$

$$\mathbf{v}_{TX2} = [0 \ +1 \ +1 \ 0 \ -1 \ -1 \ 0 \ -1 \ -1 \ 0 \ +1 \ +1]^T.$$

The corresponding receiver codes are time-shifted versions of the transmitter codes

$$\mathbf{v}_{RX1} = [-1 \ 0 \ +1 \ +1 \ 0 \ -1 \ -1 \ 0 \ +1 \ +1 \ 0 \ -1]^T,$$

$$\mathbf{v}_{RX2} = [+1 \ 0 \ +1 \ +1 \ 0 \ -1 \ -1 \ 0 \ -1 \ -1 \ 0 \ +1]^T.$$

⁷Synchronization among transceivers can be performed with additional hardware to maximize power transfer; it is straightforward to prove that codes of unrelated transceivers are shift-orthogonal.

The parameter γ for the X-CMCD hardware that can realize these two codes from the code set, is calculated iteratively by starting with a reasonably low value and increasing gradually until the two codes are realized. Recall that a code is realized when all the switch turn OFF operations lead to a half sine voltage of appropriate polarity across the WPT inductor. Using the two transmitter codes and iteratively solving for a γ that can realize both codes yields $\gamma \geq \gamma_{\min} = 0.0625$.

The model waveforms derived from the peak voltage and current values can be used to verify the orthogonality of the unrelated transceivers. Thus, any $\gamma \geq \gamma_{\min}$ can be used for the realization of a WPT network with 2 transceivers using \mathbf{v}_{TX1} and \mathbf{v}_{TX2} .

The transceiver components: power semiconductor switch, CMCD inductors L_r , and resonant capacitor C_r , together with the operating frequency can be selected by solving the optimization described in Section IV. The optimization is formulated with an objective function to minimize the sum of two loss-factors corresponding to both codes,

$$\underset{L_r, C_r}{\text{minimize}} \ell_c = \ell_1 + \ell_2, \quad (39)$$

where ℓ_1 and ℓ_2 are the loss-factors corresponding to the two codes (37). The combined loss-factor can be expressed as

$$\ell_c = \frac{(n_{Lr,1} + n_{Lr,2})}{Q_{fr}} + \frac{(n_{cd,1} + n_{cd,2}) \tau_{sw}}{\omega_r L_r C_{OSS}} + (n_{COSS,1} + n_{COSS,2}) \omega_r^2 L_r C_{OSS}. \quad (40)$$

The combined loss-factor is still convex in the variable $x = L_r C_{OSS}$ for a fixed resonant frequency ω_r . For a given device or device technology, there is a minimum C_{OSS} choice that corresponds to the smallest device; also, because of imposed limitations on physical size or intrinsic parasitics, there are upper and lower limits to the inductors that can be realized. Also, the half sine resonant frequency ω_r puts an upper bound on x . Thus, the practical constraints of the optimization can be summarized as

$$L_{r_{\min}} C_{OSS_{\min}} \leq x \leq \min \left\{ \frac{1}{\omega_r^2 l_{eq}}, L_{r_{\max}} C_{OSS_{\max}} \right\}, \quad (41)$$

where $l_{eq} = L_{eq}/L_r$. These added constraints are linear so the optimization problem remains convex and easily solvable for a chosen resonant frequency.

It may be possible to improve loss-factor by iteratively increasing $\gamma \geq \gamma_{\min}$. Fig. 18 shows the plot of the minimum loss-factor (39) for different values of γ . The value of γ that yields the minimum combined loss-factor is $\gamma_{\text{opt}} = 0.3125$ for a resonant frequency of 7.5 MHz.

For γ_{opt} , solving the optimization yields the value of $L_r C_{OSS}$ that minimizes the combined loss-factor. Based on commercially available semiconductor switches with a chosen τ_{sw} and practically realizable inductors, we can select the switch and the corresponding CMCD inductors. For example, an inductor with a value of ≈ 297 nH is required for the GaN switch GS61008P from GaN Systems, Inc. The additional

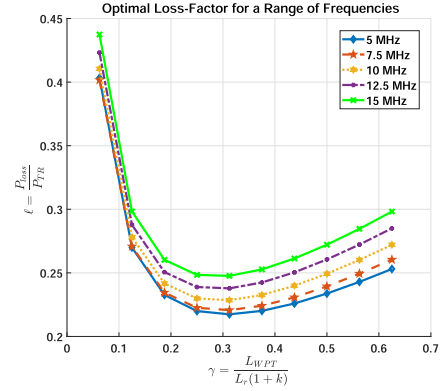


FIGURE 18. Variation of optimal loss-factor ℓ_{opt} over γ at different half sine resonant frequencies.

TABLE 1. Transceiver components for 2×2 WPT network.

Component	Value
γ	0.3125
f_r	7.5 MHz
Switch	GS61008P
L_r	297 nH
k	0.6
L_{WPT}	297 nH
C_r	465 pF

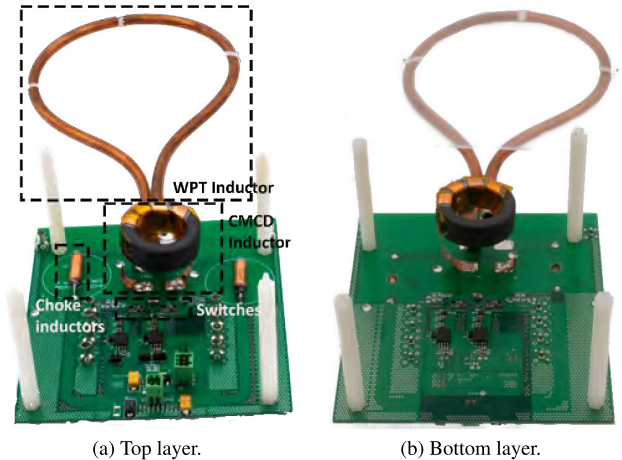


FIGURE 19. Transceiver prototype for a WPT network with four transceivers. The transceivers have components symmetrically on the top and bottom layer to minimize parasitic inductance.

resonant capacitor C_r for the CMCD subcircuit is

$$C_r = \frac{1}{\omega_r^2 L_{eq}} - C_{OSS}. \quad (42)$$

The transceiver components for an optimized 2×2 WPT network are summarized in Table 1.

B. HARDWARE RESULTS OF A CDMA-WPT NETWORK WITH FOUR TRANSCEIVERS

1) TRANSCEIVER IMPLEMENTATION

The implementation details for the transceivers of a 2×2 WPT network are given in Table 2. The CMCD inductors

TABLE 2. Implemented components for prototype transceiver.

Component	Value	Description
Gate Drivers	UCC27611	5-V, 4-A to 6-A low-side driver.
L_r	660 nH	Using single-layered foil on 5967002701 core Fair-Rite Corp.
L_{WPT}	320 nH	Single turn with 5 cm radius realized using hollow copper tubing.
C_r	220 pF	501S42E221JV3S Johanson Technology, Inc.
L_{choke}	22 μ H	EPCOS B82111E Series.
f_r	8.33 MHz	Resonant Frequency.
k_r	0.6	Coupling between CMCD tank inductors.

were realized using a 5 mil thick copper foil winding on a 67-material toroidal core from Fair-Rite Corporation; this low-permeability, high-frequency core material was used to achieve a higher coupling between the CMCD inductors and a lower overall loss (i.e., high quality factor at 8.33 MHz). As was discussed in Section III-A, the increased coupling has the advantage of higher equivalent inductance during resonance and higher voltage across the WPT inductor. The implemented γ is 0.303 which is very nearly the design optimal $\gamma_{opt} = 0.3125$. Adjustments were performed to the design parameters made to account for the non-linearity of the switches, which results in an implemented $C_r = 220$ pF, along with others to account for manufacturing precision and tolerances. Fig. 19 shows a prototype of the implemented transceiver modules. The transceivers were constructed using a four-layer PCB that has a symmetric top and bottom layer with shielding layers provided by two ground planes in the middle. This was performed to ensure minimal parasitic ringing.

2) REALIZATION OF ORTHOGONAL CODES

The implemented $\gamma = 0.303$ is larger than $\gamma_{min} = 0.0625$, hence the codes can be realized by the implemented transceiver. Fig. 20 shows the oscilloscope images for the two codes realized in hardware by two different transceivers. It can be observed from the scope waveforms that the two codes are realized with nearly identical half sine wave voltages of the same amplitude. The no-load losses corresponding to the v_{TX1} and v_{TX2} are 0.68 W and 0.69 W respectively. It is important to note that the current-mode topology allows the

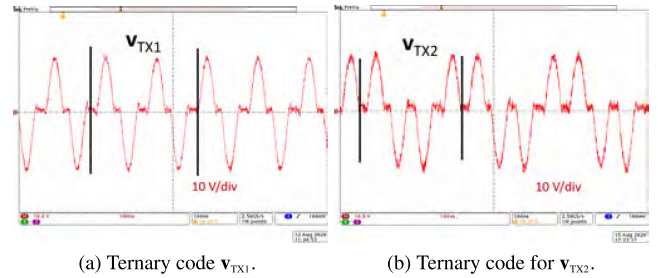


FIGURE 20. Scope waveforms of the realization of ternary codes v_{TX1} and v_{TX2} . The codes are realized with nearly ideal sine voltages of identical peak magnitudes.

TABLE 3. Hardware data for isolated TX-RX pairs of 2 x 2 WPT network.

Transceiver Arrangement	Power and Efficiency		
	P_{TX}	P_{RX}	η_{dc-dc}
RX ₁	6.54 W	-5.00 W	76.61%
RX ₂	6.63 W	-5.04 W	76.02%

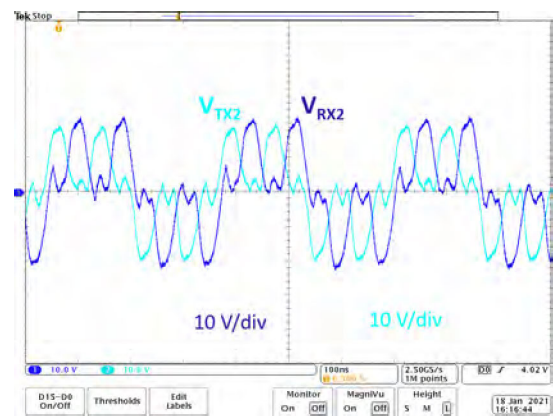


FIGURE 21. Scope waveforms of the realization of transmitter and receiver codes for a 2 x 2 WPT network. An appropriate choice of zero durations allows the receiver codes to be shifted versions of the transmitter code.

transmitters to function properly from no-load to full-load (transmitter with a coupled receiver).

3) RECEIVING POWER FROM ORTHOGONAL CODES

An isolated TX-RX pair is separated by 2.5 cm (approximately half WPT coil radius) and negligible lateral misalignment. The time-shifted transmitter codes are used as receiver codes, as shown by the scope waveforms for TX₂ and RX₂ in Fig. 21. Note that in Figs. 21 and 23 the small oscillations near the zero durations and the peaks are measurement artifacts from using single-ended probes. Table 3 summarizes the dc power data of TX and RX for the two ternary codes and their corresponding dc-to-dc efficiency. The negative sign in the receiver power indicates that the receivers provide power to the dc bus.

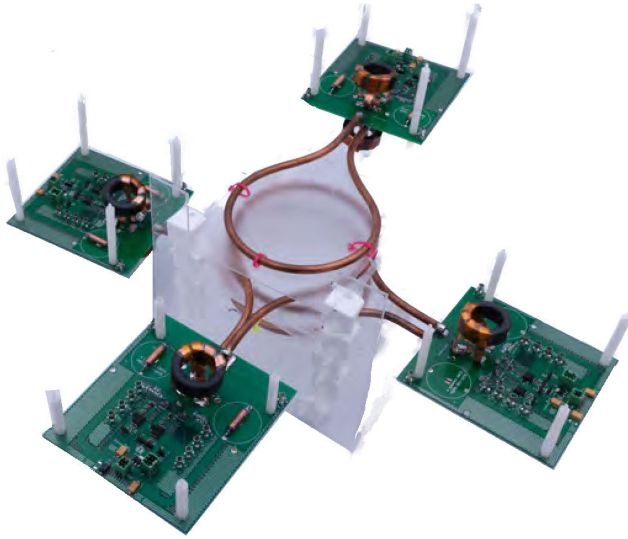


FIGURE 22. Transceiver arrangement for 2 × 2 multiple access WPT hardware data.

4) MULTIPLE ACCESS WPT

The four transceivers were then arranged so that they shared a common electromagnetic space as shown in Fig. 22 with the neighboring transceivers being separated by 2.5 cm (approximately half the WPT coil radius). The related transceivers were made to exchange power by using the appropriate ternary code. Fig. 23 shows the simultaneous realization and operation of the transmitter ternary codes v_{TX1} and v_{TX2} together with their corresponding time-shifted codes for the receivers. Compared to the waveforms in Fig. 23, simultaneous operation results in nearly imperceptible differences, which helps verify our simplifying assumptions in Section II. Table 4 shows the dc power levels and dc-dc efficiency for power exchange among the related transceivers in the different transceiver configurations. In the first configuration, the receivers are in the middle and hence are strongly coupled to each other, whereas in the fourth configuration the transmitters are strongly coupled. The second and third configurations have an unrelated TX-RX pair strongly coupled to each other. To examine the effectiveness for multiple access, the percentage interference on each transceiver is calculated as

$$\Delta P = \frac{|P^S - P^M|}{P^S}, \tag{43}$$

where P^S is the transceiver dc power in an isolated TX-RX WPT, and P^M is the transceiver dc power within multiple access. It can be observed from Table 4 that the mean power deviation is less 0.75 % than and the worst-case power deviation is approximately 1.74 % from the non-interference case over the different configurations in the shared electromagnetic space, hence achieving the practical orthogonality discussed in Section III-E. It should be pointed out that that effectiveness of multiple access depends on the realization of proper orthogonal codes by the individual transceivers. For low-loss loosely-coupled transceivers ($k < 0.4$), the output

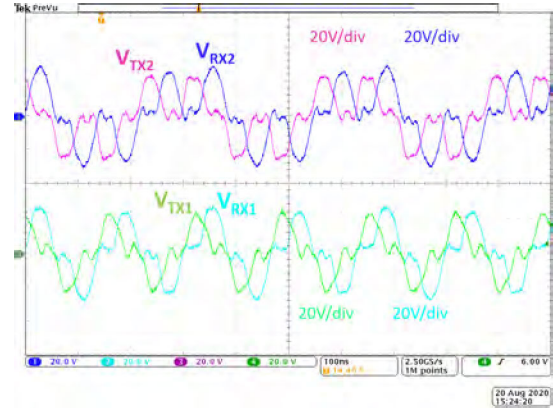


FIGURE 23. Scope waveforms for simultaneous operation of TX₁, RX₁, TX₂, and RX₂.

TABLE 4. Hardware data for a multiple access 2 × 2 WPT network.

Transceiver Arrangement		TX ₁	RX ₁	TX ₂	RX ₂
(1)	P_{dc}	6.84 W	5.20 W	6.62 W	4.92 W
	ΔP	0.03 %	0.69 %	0.22 %	1.74 %
	η_{dc-dc}	76.10 %		74.23 %	
(2)	P_{dc}	6.58 W	5.00 W	6.53 W	4.95 W
	ΔP	1.21 %	0.52 %	1.02 %	1.69 %
	η_{dc-dc}	75.90 %		75.91 %	
(3)	P_{dc}	6.78 W	5.21 W	6.70 W	5.05 W
	ΔP	0.58 %	0.85 %	0.10 %	0.95 %
	η_{dc-dc}	76.61 %		76.02 %	
(4)	P_{dc}	6.57 W	5.00 W	6.68 W	5.02 W
	ΔP	1.01 %	0.48 %	0.77 %	0.53 %
	η_{dc-dc}	75.04 %		76.03 %	

voltage closely matches the model waveforms, hence maintain practical orthogonality.

C. DESIGN OF A WPT NETWORK WITH 8 TRANSCEIVERS

Consider a design example with 8 transceivers operating as four transmitters and four receivers. At most, each transmitter can transfer power to its related receiver, thus requiring maximum of four orthogonal codes. The two orthogonal codes obtained in Section V-A are used as base codes, $\mathbf{a} = v_{TX1}$ and $\mathbf{b} = v_{TX2}$. Applying the design process, the four orthogonal codes corresponding to $\gamma_{min} = 0.375$ are obtained as

$$\begin{aligned} \mathbf{v}_{TX1} &= [\mathbf{a} \ \mathbf{a} \ \mathbf{a} \ \mathbf{a}], & \mathbf{v}_{TX2} &= [\mathbf{b} \ \mathbf{b} \ \mathbf{b} \ \mathbf{b}], \\ \mathbf{v}_{TX3} &= [\mathbf{a} \ \mathbf{a} \ \mathbf{c} \ \mathbf{c}], & \mathbf{v}_{TX4} &= [\mathbf{b} \ \mathbf{d} \ \mathbf{d} \ \mathbf{b}]. \end{aligned}$$

TABLE 5. Parameters for optimization of loss-factor.

Parameter	$Q_{Lr}(@1\text{ MHz})$	τ_{sw}	k
Value	200	2000 fs	0.6

TABLE 6. Transceiver components for WPT network with 8 transceivers.

Component	Value
γ	0.375
f_r	7.5 MHz
Switch	GS61008P
L_r	295 nH
k	0.6
L_{WPT}	375 nH
C_r	438 pF

where $\mathbf{c} = -\mathbf{a}$ and $\mathbf{d} = -\mathbf{b}$ are negative ternary codes corresponding to base codes \mathbf{a} and \mathbf{b} , respectively. Recall that the corresponding receiver codes are time-shifted versions of the transmitter codes.

To obtain the values and parameters for the transceiver components, the combined loss-factor is minimized by solving the following optimization problem,

$$\begin{aligned} &\text{minimize } l_c = l_1 + l_2 + l_3 + l_4 \\ &x=L_r C_{OSS} \\ &\text{subject to } L_{r\min} C_{OSS\min} \leq x \leq \min \left[\frac{1}{\omega_r^2 l_{eq}}, L_{r\max} C_{OSS\max} \right] \end{aligned}$$

where l_i is the loss-factor corresponding to the transceiver realizing the i^{th} transmitter code. The optimization is performed using the values and parameters in Table 5 at a resonant frequency of 7.5 MHz.

The optimal inductance L_r that minimizes the power factor with the switch GS61008P is 295 nH. The transceiver parameters that can realize four orthogonal codes are summarized in Table 6.

D. HARDWARE RESULTS OF CDMA-WPT NETWORK WITH 8 TRANSCIVERS




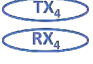
1) TRANSCIVER IMPLEMENTATION

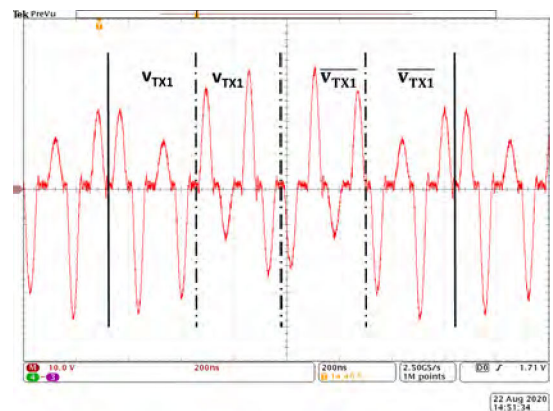
It can be observed from Table 1 and 6 that the design parameters for the transceivers of the 8 transceiver WPT network using the GS61008P GaNFET are similar to WPT network with four transceivers with the exception of the values for the WPT inductor and the resonant capacitor. A $\gamma_{opt} = 0.375$ is needed for the realization of the four ternary codes; hence, the WPT inductor was increased to $L_{WPT} = 375$ nH. Additionally, the frequency was reduced slightly to 8 MHz to ensure ZVS for all four codes.

2) REALIZATION OF TERNARY CODES

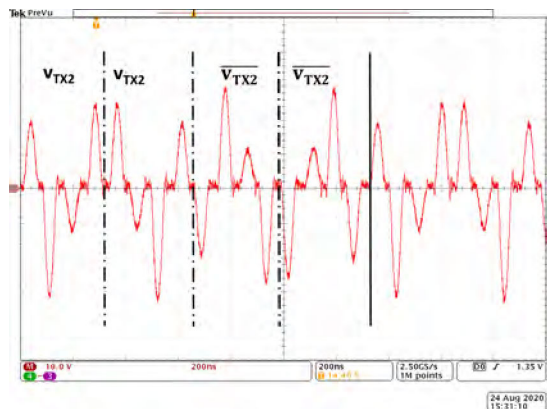
A $\gamma \geq \gamma_{min} = 0.375$ can realize the four ternary codes while ensuring their orthogonality, which means that $L_{WPT} = 375$ nH can realize all four ternary codes. Fig. 24 shows the oscilloscope waveforms for the codes v_{TX3} and v_{TX4} ; note that the waveforms for the codes v_{TX1} and v_{TX2} are identical to the codes for the 2×2 network in Fig. 20. It can

TABLE 7. Hardware data for a WPT network with 8 transceivers.

Transceiver Arrangement	Power and Efficiency		
	P_{TX}	P_{RX}	η_{dc-dc}
	4.89 W	3.78 W	77.35%
	4.91 W	3.78 W	76.99%
	5.15 W	3.8 W	73.79%
	5.41 W	4.04 W	74.62%



(a) Ternary code v_{TX3} .

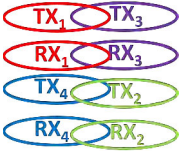
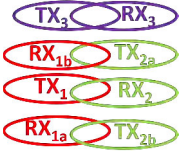


(b) Ternary code for v_{TX4} .

FIGURE 24. Oscilloscope waveforms for v_{TX3} and v_{TX4} for $\gamma = 0.375$. All of the half sine voltages are realized but with variable peak magnitudes due to an insufficient γ .

be observed that the sufficient value of $\gamma = 0.375$ prevents code-failures but is not large enough to avoid having the half sine voltages vary in peak magnitudes. The scope waveforms closely match the model waveforms with minor deviations owing to the non-linearity of the output drain capacitance of the GaN FETs.

TABLE 8. Hardware data for WPT network with 8 transceivers.

Transceiver Arrangement		TX ₁	RX ₁	TX ₂	RX ₂	TX ₃	RX ₃	TX ₄	RX ₄
(1) 	P_{dc}	5.45 W	4.21 W	4.91 W	3.74 W	5.59 W	3.98 W	5.80 W	4.24 W
	ΔP	0.01 %	5.40 %	1.58 %	5.32 %	0.01 %	4.07 %	0.01 %	1.96 %
	η_{dc-dc}	77.22 %		76.2 %		71.2 %		73.05 %	
(2) 	P_{dc}	TX ₁	RX _{1a}	RX _{1b}	TX _{2a}	TX _{2b}	RX ₂	TX ₃	RX ₃
	ΔP	8.94 W	3.63 W	3.54 W	5.24 W	5.53 W	8.16 W	6.56 W	4.77 W
	η_{dc-dc}	0.15 %	1.41 %	4.53 %	8.78 %	0.60 %	5.36 %	0.36 %	3.26 %
		80.30 %			75.70 %		72.76 %		

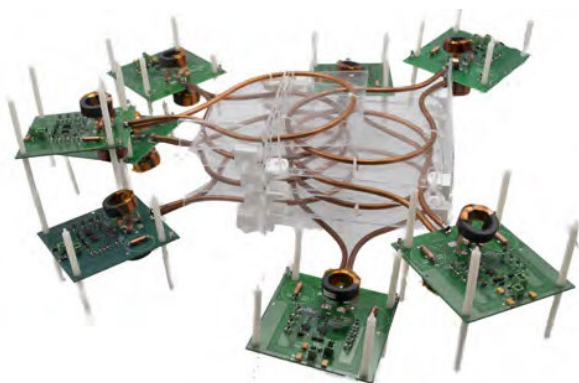


FIGURE 25. Transceiver arrangement for obtaining multiple access WPT hardware data with 8 transceivers.

3) RECEIVING POWER THROUGH TERNARY CODES

Time-shifted transmitter codes are used as the receiver codes. Each related TX-RX pair is isolated and kept 3 cm apart ($k \approx 0.32$) with minimal lateral misalignment. Table 7 shows the dc power levels and dc-to-dc efficiencies for each of the four related transceiver pairs operating in isolation. An appropriate choice of transceiver components obtained by minimizing the combined loss factor helps to ensure that the four pairs have comparable and acceptable dc-dc efficiency.

4) MULTIPLE ACCESS WPT

The eight transceivers are physically arranged in Fig. 25 for multiple access WPT with the coupling, $k \in (0.29, 0.32)$ between the related TX and RX exchanging power. Two different configurations are evaluated for demonstrating effective multiple access. In the first configuration, the four orthogonal codes are assigned to four related TX-RX pairs forming a 4×4 WPT network, and other configuration consists of a SIMO, MISO and a SISO systems with three orthogonal codes to form a complex WPT network.

Table 8 shows the results for a few representative configurations of the WPT network together with the dc power

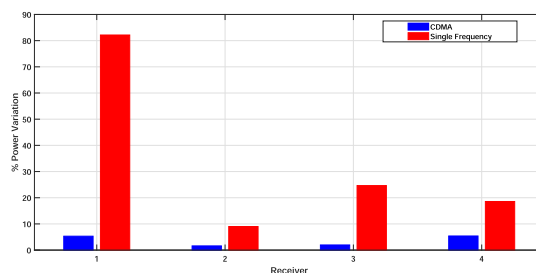


FIGURE 26. Comparison of receiver power variation for the transceiver arrangement in Fig. 25 operating as four TX-RX pairs.

level and dc-dc efficiency of each related transceiver pair. It can be observed that the maximum deviation because of interference in power level remains within 9 % of the power level in isolation (no interference) with a mean interference of 1.81 % over different configurations, hence achieving practical orthogonality. In comparison, when operated at single frequency as four TX-RX pairs, the interference in power level is up to 82 % as illustrated in Fig. 26 as well as the attached media with paper.

VI. CONCLUSION

Wireless Power Transfer (WPT) is the key to unlocking the potential of densely connected networks of devices. Powering these networks requires efficient mutable multiple access WPT. The important characteristics of multiple access WPT are power flow selectivity and scalability. In this paper, we presented an implementation of CDMA-WPT that enables mutable multiple access WPT while maintaining power flow selectivity and ease of scalability. CDMA exploits orthogonality in code space to enable multiple access. An encoding scheme for abstracting the outputs of quasi-resonant converters as ternary (three-level) codes, the power flow model, and a code construction algorithm for scaling to large number of TX-RX pairs were also presented. In the future, orthogonal codes can be designed to satisfy regulatory electromagnetic interference (EMI) constraints.

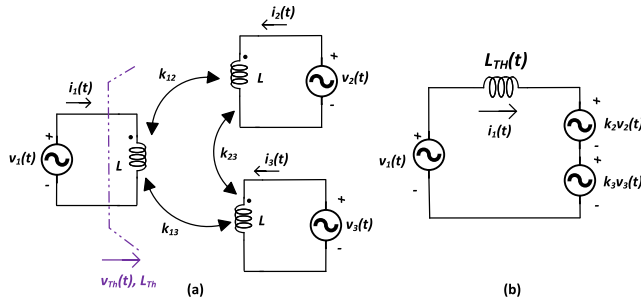


FIGURE 27. WPT system with three transceivers having the voltage sources v_1 , v_2 , and v_3 driving identical coupled inductors. The power flow from v_1 can be obtained from the Thevenin equivalent voltage and inductance at the terminals of its WPT inductor, which becomes the simplified voltage source model.

The hardware implementation of CDMA-WPT is presented using a new quasi-resonant converter capable of operating as an inverter or rectifier. The time-domain analysis required for analyzing the performance during the realization of different codes was also presented along with a design process for practical co-design of high-performance hardware and obtaining a code set. The application of CDMA-WPT was demonstrated in hardware using four transceivers maintaining a nearly constant 5 W operation with 75 % dc-dc efficiency between two TX-RX pairs, and eight transceivers in different configurations maintaining a nearly constant 4 W operating with more than 71 % dc-dc efficiency while maintaining power flow selectivity.

**APPENDIX A
VOLTAGE SOURCE MODEL FOR WIRELESS POWER TRANSFER**

Consider the WPT system shown in Fig. 27 with three voltage sources driving coupled identical inductors with coupling coefficients k_{12} , k_{13} , and k_{23} . To obtain the power flowing out of v_1 , the Thevenin equivalent circuit at the terminals of v_1 is derived. For lossless inductors, the voltages and currents for the three transceivers are related by

$$\begin{bmatrix} v_1 \\ v_2 \\ v_3 \end{bmatrix} = L \begin{bmatrix} 1 & k_{12} & k_{13} \\ k_{12} & 1 & k_{23} \\ k_{13} & k_{23} & 1 \end{bmatrix} \frac{d}{dt} \begin{bmatrix} i_1 \\ i_2 \\ i_3 \end{bmatrix}, \quad (44)$$

where k_{ij} is the coupling coefficient between the i^{th} and j^{th} transceiver, and L is the self-inductance of the identical transceivers. The Thevenin equivalent voltage is obtained by finding the open-circuit voltage at the terminals of the WPT inductor of Transceiver 1,

$$v_{Th} = \underbrace{\frac{(k_{12} - k_{23}k_{13})}{1 - k_{23}^2}}_{k_2} v_2 + \underbrace{\frac{(k_{13} - k_{23}k_{12})}{1 - k_{23}^2}}_{k_3} v_3, \quad (45)$$

and the Thevenin inductance is obtained across the same terminals by short-circuiting the sources v_2 and v_3 ,

$$L_{Th} = \left(1 - \frac{(k_{12}^2 + k_{13}^2 - 2k_{23}k_{12}k_{13})}{1 - k_{23}^2} \right) L. \quad (46)$$

Thus, the Thevenin equivalent circuit at terminals of v_1 reduces to a two-bus voltage source model with v_{Th} as the other voltage source and L_{Th} as the connecting impedance. It is worth noting that for $k_{13} = k_{23} = 0$, the Thevenin circuit reduces to the conventional two-voltage source model for WPT with

$$v_{Th} = k_{12}v_2 \quad (47)$$

$$L_{Th} = (1 - k_{12}^2)L. \quad (48)$$

In general, a WPT system with any number of transceivers can also be proven similarly to reduce to a two-bus voltage source model for obtaining the power flow for each transceiver.

**APPENDIX B
CODE CONSTRUCTION ALGORITHM FOR SCALING WPT**

Algorithm 2: Obtaining N Orthogonal Codes

```

Result: Obtain at least  $N$  orthogonal codes
Start with a set of 2 orthogonal codes,  $\mathcal{S}_1 = \{\mathbf{c}_1, \mathbf{c}_2\}$  of length  $2^k$   $i = 1$ ;
while  $i \leq \log_2 N - 1$  do
    Construct codes of length  $2^{k+1}$  by concatenating set  $\mathcal{S}_i$  with itself and  $\mathcal{S}_i$  with  $-\mathcal{S}_i$ ;
     $\mathcal{S}_{i+1} = \{\mathcal{S}_i \sqcup \mathcal{S}_i, \mathcal{S}_i \sqcup -\mathcal{S}_i\}$ ;
     $i = i + 1$ ;
end
    
```

The code construction algorithm (CCA) can be used to obtain orthogonal codes for scaling CDMA-WPT. The CCA starts with a set of two orthogonal ternary codes, $\mathcal{S}_1 = \{\mathbf{c}_1, \mathbf{c}_2\}$. These two codes can be obtained by starting with an initial ternary code and solving the optimization problem (16) to obtain the second orthogonal code. In the next step, the CCA constructs more codes using the set concatenation operation. The set concatenation operation (\sqcup) is an element wise concatenation operation of the ternary codes that increases the lengths of the ternary codes by increasing the code period. Consider two sets of ternary codes, $\mathcal{S}_a = \{\mathbf{a}_1, \mathbf{a}_2, \dots, \mathbf{a}_N\}$ and $\mathcal{S}_b = \{\mathbf{b}_1, \mathbf{b}_2, \dots, \mathbf{b}_N\}$ having an equal number of valid codes N with code periods, T_A and T_B , respectively. The concatenation of these two sets is defined as

$$\mathcal{S}_c = \mathcal{S}_a \sqcup \mathcal{S}_b \triangleq \{\mathbf{a}_1\mathbf{b}_1, \mathbf{a}_2\mathbf{b}_2, \mathbf{a}_3\mathbf{b}_3, \dots, \mathbf{a}_N\mathbf{b}_N\}. \quad (49)$$

The ternary codes of the concatenated set \mathcal{S}_c have a code period $T_A + T_B$. An orthogonal set \mathcal{S}_k with N codes when concatenated with itself and its negative $-\mathcal{S}_k$ leads to a set \mathcal{S}_{k+1} with $2N$ orthogonal codes [47]. CCA uses repeated concatenation operations to obtain the desired number of orthogonal codes.

The CCA algorithm thus increases the code length to obtain more orthogonal codes. As the code length increases, so does the code period. Hence, the instantaneous power flow oscillates with a longer period. Consider the two orthogonal codes, v_1 and v_2 obtained in the previous section as initial

codes. Applying CCA with the initial set $\mathcal{S}_1 = \{\mathbf{v}_1, \mathbf{v}_2\}$ results in set \mathcal{S}_2 with four orthogonal codes

$$\mathcal{S}_2 = \{\mathbf{v}_1\mathbf{v}_1, \mathbf{v}_2\mathbf{v}_2, \mathbf{v}_1\overline{\mathbf{v}_1}, \mathbf{v}_2\overline{\mathbf{v}_2}\},$$

where $\overline{\mathbf{v}_1} = -\mathbf{v}_1$ and $\overline{\mathbf{v}_2} = -\mathbf{v}_2$. Because the codes are periodic, the codes $\mathbf{v}_1\mathbf{v}_1$ and $\mathbf{v}_2\mathbf{v}_2$ behave identically to the initial codes \mathbf{v}_1 and \mathbf{v}_2 . We assign these four codes to four transceivers $\{\text{TX}_1, \dots, \text{TX}_4\}$.

APPENDIX C ESTIMATING TRANSCIEVER PERIODIC STEADY-STATE CURRENTS

The steady state voltages and currents for an X-CMCD transceiver can be obtained from linear equations describing the fundamental power electronics properties. In this section we describe a method for estimating the X-CMCD waveforms. For a lossless transceiver, the energy at the end of a code is the same as at the beginning. Similarly, the energy is conserved during the realization of a polarity from the beginning to the end. Thus, the current distribution at the end of the polarity is related to the current at the beginning of the polarity

$$\mathbf{i}[j+1] = \mathbf{A}_j \mathbf{i}[j], \quad (50)$$

where \mathbf{A}_j is the current evolution matrix that depends on the switch states. Equation (59) can be applied iteratively to obtain

$$\mathbf{i}[N+1] = \mathbf{A}_N \mathbf{A}_{N-1} \dots \mathbf{A}_1 \mathbf{i}[1]. \quad (51)$$

Equation (58) and (60) can now be combined to obtain

$$\mathbf{A}_C \mathbf{i}[1] = 0, \quad (52)$$

where $\mathbf{A}_C = \mathbf{A}_N \mathbf{A}_{N-1} \dots \mathbf{A}_1$ is a matrix that depends on the switching sequence and hence the entire ternary code being realized by the transceiver; note that $\mathbf{i}[1]$ is the inductor current distribution vector at the beginning of the ternary code.

During the realization of a positive polarity, v_P is related to the voltage of the resonating capacitor in CMCD-1

$$v_P = \frac{\gamma(1+k) + \frac{1}{4}(1-k)}{\gamma(1+k) + \frac{1}{2}(1-k)} \frac{v_C}{2}, \quad (53)$$

and v_N is

$$v_N = \frac{\frac{1}{4}(1-k)}{\gamma(1+k) + \frac{1}{2}(1-k)} \frac{v_C}{2}, \quad (54)$$

where k is the coupling between the inductors within the same CMCD subcircuit. It is worth noting that for perfectly coupled CMCD inductors ($k = 1$), v_N will be zero during the realization of a positive polarity. The capacitor voltage, v_C is related to the current at the beginning of the polarity from (26). Thus, the peak voltage of v_P and v_N during the realization of a positive and negative polarity is related to the current in the inductors of CMCD-1 and CMCD-2, respectively, at the beginning of a polarity.

Using (62), (63), and (59), another set of equations can be obtained to solve for $\mathbf{i}[1]$ at the beginning of the ternary code,

$$\mathbf{A}_V \mathbf{i}[1] = V_{dc} \quad (55)$$

where \mathbf{A}_V is a matrix that depends on the ternary code. Equations (61) and (64) can be used to solve for $\mathbf{i}[1]$, the steady-state inductor current distribution at the beginning of the ternary code. Once the initial current distribution $\mathbf{i}[1]$ is obtained, it can be used for calculating the voltage and current waveforms, called the *model waveforms* for the entire code. In order to analyze and design an X-CMCD transceiver, the estimation of the currents and voltages in steady-state is needed. The periodic steady-state currents and voltages for an X-CMCD transceiver depends on the ternary code (hence, the switching sequence) realized by the transceiver. A ternary code is said to be realized by the transceiver if all the switching operations lead to the realization of a half sine voltage. The peak magnitude of these half sine voltages are related to the current distribution among inductors in (26). As discussed in the next section, if the current in the corresponding inductor is negative before the operation of the switch, then the switching operation will not lead to the creation of a half sine voltage and would result in a *code-failure*. We can use a circuit simulator like LTSpice to predict the realization of a code; however, simulating the transceiver for every ternary code may be impractical. Alternatively, approximate voltage and current waveforms can also be obtained by solving the steady-state linear equations for lossless transceivers utilizing two properties:

- 1) *Inductor volt-second balance across the choke inductors*: The average voltage across the choke inductors is zero over the code period for inductor volt-second balance [53],

$$V_{dc} = \frac{1}{T} \int_0^T v_p(t) dt = \frac{1}{T} \int_0^T v_n(t) dt, \quad (56)$$

where T is the code period; $v_p(t)$ and $v_n(t)$ are the voltages of the WPT inductor nodes as illustrated in Fig. 10. If we assume the transceiver voltages are sinusoidal, (56) can be simplified to

$$V_{dc} = \frac{2T_P}{T\pi} \sum_{i=1}^M v_{pk}^P[i] = \frac{2T_P}{T\pi} \sum_{i=1}^M v_{pk}^N[i], \quad (57)$$

where D is the duty-cycle, M is the number of polarities in the ternary code; $v_{pk}^P[i]$ and $v_{pk}^N[i]$ are the peak voltages of v_P and v_N , respectively, during the realization of the i^{th} polarity.

- 2) *Periodicity of currents over the code period*: Another condition for the realization of a code by the transceiver is that the transceiver currents and voltages are periodic in the steady state over the code period. Hence, for a ternary code with M polarities, the inductor currents must be identical at the beginning and the end of the code

$$\mathbf{i}[M+1] = \mathbf{i}[1], \quad (58)$$

where $\mathbf{i}[j] = [i_1^P \ i_2^P \ i^{\text{WPT}} \ i_1^N \ i_2^N]^T$ is the current vector before the realization of j^{th} polarity, i.e. $i_k^X = i_k^X[n]$.

For a lossless transceiver, the energy at the end of a code is the same as at the beginning. Similarly, the energy is conserved during the realization of a polarity from the beginning to the end. Thus, the current distribution at the end of the polarity is related to the current at the beginning of the polarity

$$\mathbf{i}[j+1] = \mathbf{A}_j \mathbf{i}[j]. \quad (59)$$

where \mathbf{A}_j is the current evolution matrix that depends on the switch states. Equation (59) can be applied iteratively to obtain

$$\mathbf{i}[N+1] = \mathbf{A}_N \mathbf{A}_{N-1} \dots \mathbf{A}_1 \mathbf{i}[1]. \quad (60)$$

Equation (58) and (60) can now be combined to obtain

$$\mathbf{A}_C \mathbf{i}[1] = 0, \quad (61)$$

where $\mathbf{A}_C = \mathbf{A}_N \mathbf{A}_{N-1} \dots \mathbf{A}_1$ is a matrix that depends on the switching sequence and hence the entire ternary code being realized by the transceiver; note that $\mathbf{i}[1]$ is the inductor current distribution vector at the beginning of the ternary code.

During the realization of a positive polarity, v_P is related to the voltage of the resonating capacitor in CMCD-1

$$v_P = \frac{\gamma(1+k) + \frac{1}{4}(1-k) v_C}{\gamma(1+k) + \frac{1}{2}(1-k) 2}, \quad (62)$$

and v_N is

$$v_N = \frac{\frac{1}{4}(1-k)}{\gamma(1+k) + \frac{1}{2}(1-k) 2} v_C, \quad (63)$$

where k is the coupling between the inductors within the same CMCD subcircuit. It is worth noting that for perfectly coupled CMCD inductors ($k = 1$), v_N will be zero during the realization of a positive polarity. The capacitor voltage, v_C is related to the current at the beginning of the polarity from (26). Thus, the peak voltage of v_P and v_N during the realization of a positive and negative polarity is related to the current in the inductors of CMCD-1 and CMCD-2, respectively, at the beginning of a polarity.

Using (62), (63), and (59), another set of equations can be obtained to solve for $\mathbf{i}[1]$ at the beginning of the ternary code,

$$\mathbf{A}_V \mathbf{i}[1] = V_{dc} \quad (64)$$

where \mathbf{A}_V is a matrix that depends on the ternary code. Equations (61) and (64) can be used to solve for $\mathbf{i}[1]$, the steady-state inductor current distribution at the beginning of the ternary code. Once the initial current distribution $\mathbf{i}[1]$ is obtained, it can be used for calculating the voltage and current waveforms, called the *model waveforms* for the entire code.

ACKNOWLEDGMENT

The authors would like to thank Dr. Aaron Stein for his guidance on realizing inductors and A. Simha Modugala for his assistance with Verilog programming of the FPGA.

REFERENCES

- [1] J. Huh, S. W. Lee, W. Y. Lee, G. H. Cho, and C. T. Rim, "Narrow-width inductive power transfer system for online electrical vehicles," *IEEE Trans. Power Electron.*, vol. 26, no. 12, pp. 3666–3679, Dec. 2011.
- [2] A. U. Ibrahim, W. Zhong, and M. D. Xu, "A 50-kW three-channel wireless power transfer system with low stray magnetic field," *IEEE Trans. Power Electron.*, vol. 36, no. 9, pp. 9941–9954, Sep. 2021.
- [3] P. Si, A. P. Hu, S. Malpas, and D. Budgett, "A frequency control method for regulating wireless power to implantable devices," *IEEE Trans. Biomed. Circuits Syst.*, vol. 2, no. 1, pp. 22–29, Mar. 2008.
- [4] X. Dai, J. Wu, J. Jiang, R. Gao, and U. K. Madawala, "An energy injection method to improve power transfer capability of bidirectional WPT system with multiple pickups," *IEEE Trans. Power Electron.*, vol. 36, no. 5, pp. 5095–5107, May 2021.
- [5] W. M. Ng, C. Zhang, D. Lin, and S. Y. R. Hui, "Two- and three-dimensional omnidirectional wireless power transfer," *IEEE Trans. Power Electron.*, vol. 29, no. 9, pp. 4470–4474, Sep. 2014.
- [6] S. Ito, Y. Tsuchida, and M. Fukui, "An implementation of wireless power transfer system for multiple receivers," in *Proc. IEEE Int. Conf. Consum. Electron. (ICCE)*, Jan. 2019, pp. 1–4.
- [7] X. Chen, S. Yu, and Z. Zhang, "A receiver-controlled coupler for multiple output wireless power transfer applications," *IEEE Trans. Circuits Syst. I, Reg. Papers*, vol. 66, no. 11, pp. 4542–4552, Nov. 2019.
- [8] S. B. Lee and I. G. Jang, "Coil layout optimization for maximizing the power transfer efficiency of wireless power transfer systems with multiple transmitter coils," *IEEE J. Emerg. Sel. Topics Power Electron.*, vol. 8, no. 3, pp. 2672–2681, Sep. 2020.
- [9] D.-H. Kim and D. Ahn, "Maximum efficiency point tracking for multiple-transmitter wireless power transfer," *IEEE Trans. Power Electron.*, vol. 35, no. 11, pp. 11391–11400, Nov. 2020.
- [10] Y. Zhao, X. Li, Y. Ji, and C.-Z. Xu, "Random energy beamforming for magnetic MIMO wireless power transfer system," *IEEE Internet Things J.*, vol. 7, no. 3, pp. 1773–1787, Mar. 2020.
- [11] G. Ma, J. Xu, Y. Zeng, and M. R. V. Moghadam, "A generic receiver architecture for MIMO wireless power transfer with nonlinear energy harvesting," *IEEE Signal Process. Lett.*, vol. 26, no. 2, pp. 312–316, Feb. 2019.
- [12] S. Y. R. Hui and W. W. C. Ho, "A new generation of universal contactless battery charging platform for portable consumer electronic equipment," *IEEE Trans. Power Electron.*, vol. 20, no. 3, pp. 620–627, May 2005.
- [13] T. Deyle and M. Reynolds, "Surface based wireless power transmission and bidirectional communication for autonomous robot swarms," in *Proc. IEEE Int. Conf. Robot. Autom.*, May 2008, pp. 1036–1041.
- [14] J. Wang, Z. Liang, and Z. Zhang, "Energy-encrypted contactless charging for swarm robots," in *Proc. IEEE Int. Magn. Conf. (INTERMAG)*, Apr. 2017, p. 1.
- [15] Y. Yao, Z. Zhu, S. Huang, X. Yue, C. Pan, and X. Li, "Energy efficiency characterization in heterogeneous IoT system with UAV swarms based on wireless power transfer," *IEEE Access*, vol. 8, pp. 967–979, 2020.
- [16] Wireless Power Consortium, "The Qi wireless power transfer system, power class 0 specification; part 4: Reference designs," *Wireless Power Consortium*, vol. 1, p. 2017, Feb. 2016.
- [17] A. Pacini, A. Costanzo, S. Aldhafer, and P. D. Mitcheson, "Load- and position-independent moving MHz WPT system based on GaN-distributed current sources," *IEEE Trans. Microw. Theory Techn.*, vol. 65, no. 12, pp. 5367–5376, Dec. 2017.
- [18] J. Jadidian and D. Katabi, "Magnetic MIMO: How to charge your phone in your pocket," in *Proc. 20th Annu. Int. Conf. Mobile Comput. Netw.*, Sep. 2014, pp. 495–506.
- [19] D. Lin, C. Zhang, and S. Y. R. Hui, "Mathematical analysis of omnidirectional wireless power transfer—Part-I: Two-dimensional systems," *IEEE Trans. Power Electron.*, vol. 32, no. 1, pp. 625–633, Jan. 2016.
- [20] D. Lin, C. Zhang, and S. Y. R. Hui, "Mathematical analysis of omnidirectional wireless power transfer—Part-II three-dimensional systems," *IEEE Trans. Power Electron.*, vol. 32, no. 1, pp. 613–624, Jan. 2016.

- [21] L. Shi, "Orientation-independent wireless charging of multiple mobile devices at a distance," Ph.D. dissertation, Massachusetts Inst. Technol., Cambridge, MA, USA, 2016.
- [22] E. S. Lee, Y. H. Sohn, B. G. Choi, S. H. Han, and C. T. Rim, "A modularized IPT with magnetic shielding for a wide-range ubiquitous Wi-power zone," *IEEE Trans. Power Electron.*, vol. 33, no. 11, pp. 9669–9690, Nov. 2018.
- [23] B. Lee, D. Ahn, and M. Ghovanloo, "Three-phase time-multiplexed planar power transmission to distributed implants," *IEEE Trans. Emerg. Sel. Top. Power Electron.*, vol. 4, no. 1, pp. 263–272, Mar. 2015.
- [24] D. Ahn and S. Hong, "Effect of coupling between multiple transmitters or multiple receivers on wireless power transfer," *IEEE Trans. Ind. Electron.*, vol. 60, no. 7, pp. 2602–2613, Jul. 2012.
- [25] D. Ahn and S. Hong, "Effect of coupling between multiple transmitters or multiple receivers on wireless power transfer," *IEEE Trans. Ind. Electron.*, vol. 60, no. 7, pp. 2602–2613, Jul. 2013.
- [26] Y.-J. Kim, D. Ha, W. J. Chappell, and P. P. Irazoqui, "Selective wireless power transfer for smart power distribution in a miniature-sized multiple-receiver system," *IEEE Trans. Ind. Electron.*, vol. 63, no. 3, pp. 1853–1862, Mar. 2015.
- [27] A. M. Jawad, H. M. Jawad, R. Nordin, S. K. Gharghan, N. F. Abdullah, and M. J. Abu-Alshaer, "Wireless power transfer with magnetic resonator coupling and sleep/active strategy for a drone charging station in smart agriculture," *IEEE Access*, vol. 7, pp. 139839–139851, 2019.
- [28] K. E. Koh, T. C. Beh, T. Imura, and Y. Hori, "Impedance matching and power division using impedance inverter for wireless power transfer via magnetic resonant coupling," *IEEE Trans. Ind. Appl.*, vol. 50, no. 3, pp. 2061–2070, May/Jun. 2014.
- [29] M. Fu, T. Zhang, P. C.-K. Luk, X. Zhu, and C. Ma, "Compensation of cross coupling in multiple-receiver wireless power transfer systems," *IEEE Trans. Ind. Informat.*, vol. 12, no. 2, pp. 474–482, Apr. 2016.
- [30] J. Kim, H.-C. Son, D.-H. Kim, and Y.-J. Park, "Optimal design of a wireless power transfer system with multiple self-resonators for an LED TV," *IEEE Trans. Consum. Electron.*, vol. 58, no. 3, pp. 775–780, Aug. 2012.
- [31] G. Yang, M. R. V. Moghadam, and R. Zhang, "Magnetic MIMO signal processing and optimization for wireless power transfer," *IEEE Trans. Signal Process.*, vol. 65, no. 11, pp. 2860–2874, Jun. 2017.
- [32] K. Kim, H.-J. Kim, and J.-W. Choi, "Magnetic beamforming with non-coupling coil pattern for high efficiency and long distance wireless power transfer," in *Proc. IEEE Wireless Power Transf. Conf. (WPTC)*, May 2017, pp. 1–4.
- [33] L. Shi, Z. Kabelac, D. Katabi, and D. Perreault, "Wireless power hotspot that charges all of your devices," in *Proc. 21st Annu. Int. Conf. Mobile Comput. Netw.*, Sep. 2015, pp. 2–13.
- [34] W. Cai, D. Ma, X. Lai, K. Hashmi, H. Tang, and J. Xu, "Time-sharing control strategy for multiple-receiver wireless power transfer systems," *Energies*, vol. 13, no. 3, p. 599, Jan. 2020.
- [35] S. Ge, W. Liao, Q. Zhang, L. Jian, and Y. Chen, "Frequency-division technique for simultaneous wireless power transfer to two receivers," in *Proc. IEEE Int. Conf. Comput. Electromagn. (ICCEM)*, Feb. 2016, pp. 127–128.
- [36] Z. Zhang, X. Li, H. Pang, H. Komurcugil, Z. Liang, and R. Kennel, "Multiple-frequency resonating compensation for multichannel transmission of wireless power transfer," *IEEE Trans. Power Electron.*, vol. 36, no. 5, pp. 5169–5180, May 2021.
- [37] M. Haddad, P. Muhlethaler, A. Laouiti, and L. A. Saidane, "A centralized TDMA based scheduling algorithm for real-time communications in vehicular ad hoc networks," in *Proc. 24th Int. Conf. Softw., Telecommun. Comput. Netw. (SoftCOM)*, Sep. 2016, pp. 1–6.
- [38] R. Zhang, X. Cheng, L. Yang, X. Shen, and B. Jiao, "A novel centralized TDMA-based scheduling protocol for vehicular networks," *IEEE Trans. Intell. Transp. Syst.*, vol. 16, no. 1, pp. 411–416, Feb. 2014.
- [39] Z. Zhang, K. T. Chau, C. Qiu, and C. Liu, "Energy encryption for wireless power transfer," *IEEE Trans. Power Electron.*, vol. 30, no. 9, pp. 5237–5246, Sep. 2015.
- [40] X. Tian, K. T. Chau, W. Liu, and C. H. T. Lee, "Selective wireless power transfer using magnetic field editing," *IEEE Trans. Power Electron.*, vol. 36, no. 3, pp. 2710–2719, Mar. 2021.
- [41] A. Banerjee, A.-T. Avestruz, K. Surakitbovorn, A. H. Chang, and S. B. Lee, "Uniform single-sided induction heating using multiphase, multi-resonant Halbach windings," in *Proc. IEEE Appl. Power Electron. Conf. Expo. (APEC)*, Mar. 2014, pp. 844–851.
- [42] J. D. Bennett, "Spread spectrum wireless resonant power delivery," US Patent App. 12 241 268, Feb. 11, 2010.
- [43] A. Sarin and A.-T. Avestruz, "Scaling wireless power transfer through code division multiple access," in *Proc. IEEE PELS Workshop Emerg. Technol., Wireless Power Transf. (WOW)*, Jun. 2018, pp. 1–6.
- [44] A. Sarin and A.-T. Avestruz, "Active segregated inductor for code division multiple access wireless power transfer," in *Proc. 20th Workshop Control Modeling Power Electron. (COMPEL)*, Jun. 2019, pp. 1–8.
- [45] K. Shubhanga, *Power System Analysis: A Dynamic Perspective*. London, U.K.: Pearson, 2018.
- [46] H. W. Alt, *Linear Functional Analysis: An Application-Oriented Introduction*. Berlin, Germany: Springer, 1992.
- [47] A. Sarin and A.-T. Avestruz, "Code division multiple access wireless power transfer for energy sharing in heterogeneous robot swarms," *IEEE Access*, vol. 8, pp. 132121–132133, 2020.
- [48] A. Sarin, X. Cui, and A.-T. Avestruz, "Comparison of switched receivers for direct-sequence spread-spectrum wireless power transfer," in *Proc. IEEE 18th Workshop Control Modeling Power Electron. (COMPEL)*, Jul. 2017, pp. 1–8.
- [49] X. Zan and A.-T. Avestruz, "Wireless power transfer for implantable medical devices using piecewise resonance to achieve high peak-to-average power ratio," in *Proc. IEEE 18th Workshop Control Modeling Power Electron. (COMPEL)*, Jul. 2017, pp. 1–8.
- [50] K. Venkatachalam, C. R. Sullivan, T. Abdallah, and H. Tacca, "Accurate prediction of ferrite core loss with nonsinusoidal waveforms using only Steinmetz parameters," in *Proc. IEEE Workshop Comput. Power Electron.*, Jun. 2002, pp. 36–41.
- [51] G. Zulauf, S. Park, W. Liang, K. N. Surakitbovorn, and J. Rivas-Davila, "Coss losses in 600 V GaN power semiconductors in soft-switched, high- and very-high-frequency power converters," *IEEE Trans. Power Electron.*, vol. 33, no. 12, pp. 10748–10763, Dec. 2018.
- [52] J. Zhuang, G. Zulauf, J. Roig, J. D. Plummer, and J. Rivas-Davila, "An investigation into the causes of Coss losses in GaN-on-Si HEMTs," in *Proc. 20th Workshop Control Modeling Power Electron. (COMPEL)*, Jun. 2019, pp. 1–7.
- [53] R. W. Erickson and D. Maksimovic, *Fundamentals of Power Electronics*. New York, NY, USA: Springer, 2007.



AKSHAY SARIN (Member, IEEE) received the B.Tech. degree in electrical engineering from the Indian Institute of Technology Roorkee, and the M.S. and Ph.D. degrees in electrical and computer engineering from the University of Michigan, Ann Arbor, in 2017 and 2021, respectively. He is currently working as a Power Electronics Engineer with the Fuel Cell Applications Team, General Motors. His research interests include modeling and control of power electronics.



AL-THADDEUS AVESTRUZ (Member, IEEE) received the B.S. degree in physics and electrical engineering from Massachusetts Institute of Technology, Cambridge, MA, USA, and the M.S. degree in electrical engineering and the Ph.D. degree in electrical engineering and computer science from Massachusetts Institute of Technology, in 2006 and 2016, respectively. He has over a decade of industry and entrepreneurial experience. He is currently an Assistant Professor in electrical and computer engineering with the University of Michigan, Ann Arbor, MI, USA. He holds ten issued U.S. patents. His research interests include the design, modeling, and control of high-performance power electronics and wireless power transfer for energy, mobility, medicine, and the Internet of Things. He has complementary interests in circuits and systems for sensing, electromagnetic systems, feedback and controls, renewable energy, automotive, biomedical, and consumer applications. He was a recipient of the IEEE PELS Best ECCE Paper on Emerging Technology Award Oral Presentation, in 2019. He is the Chair of TC1: Control and Modeling of Power Electronics for the IEEE Power Electronics Society. He is the Associate Technical Program Chair for the IEEE Energy Conversion Congress and Exposition, in 2019, the Technical Program Co-Chair for the 2021 IEEE Wireless Power Week, and the General Chair for the 24th IEEE Workshop on Control and Modeling for Power Electronics, in 2023. He is an Associate Editor of the IEEE OPEN JOURNAL OF POWER ELECTRONICS and a Guest Associate Editor of the IEEE JOURNAL OF EMERGING AND SELECTED TOPICS IN POWER ELECTRONICS.

•••